Recent Notable Approaches to Study Self-Assembly of Nanoparticles with X-ray Scattering and Electron Microscopy

Florian Schulz, Irina Lokteva, Wolfgang J. Parak, and Felix Lehmkühler**

Dr. Florian Schulz, Dr. Irina Lokteva, Prof. Wolfgang J. Parak, Dr. Felix Lehmkühler
The Hamburg Centre for Ultrafast Imaging, 22761 Hamburg, Germany

Dr. Florian Schulz, Prof. Wolfgang J. Parak
University of Hamburg, Institute of Nanostructure and Solid State Physics, Luruper Chaussee 149, 22761 Hamburg, Germany

E-Mail: florian.schulz@physik.uni-hamburg.de

Dr. Irina Lokteva, Dr. Felix Lehmkühler
Deutsches Elektronen-Synchrotron DESY, Notkestr. 85, 22607, Hamburg, Germany

E-Mail: felix.lehmkuehler@desy.de

Keywords: self-assembly, nanoparticles, electron microcopy, x-ray scattering

Self-assembly of nanoparticles has evolved into a powerful tool for the synthesis of superstructures with tailored properties. The quality, diversity and complexity of synthesized structures is continuously improving and fascinating new collective properties have been demonstrated. At the same time, the rapid development of electron microscopy and synchrotron sources for X-rays has enabled new exciting experimental approaches to study structure and structure formation in the context of NP self-assembly. In this review we highlight and discuss some recent studies and what can be learned from them. We start with a general introduction covering important concepts, experimental approaches and commonly obtained structures and discuss the ideas of artificial atoms and emerging properties. We then present recent experimental in situ and ex situ approaches with state-of-the-art electron microscopy and X-ray diffraction and scattering that helped to obtain a detailed picture of NP self-assembly processes and resulting structures.

1 Introduction

Since the early demonstrations of nanoparticle (NP) self-assembly into supercrystals,[1] numerous intriguing structures have been reported, assembled from all kinds of NP shapes and materials into various crystals structures. Since then, the theoretical understanding of the complex interplay of involved forces has ever been improved.[2] Until today, however, there are several issues far from being resolved: for many systems long range periodic order is not routinely achieved, reproducibility is often not optimal and truly emergent and new properties arising from the supercrystal formation could be demonstrated for just a few systems.[3–7] From the materials science perspective there is no established figure of merit or common set of parameters allowing to quantify "quality" of NP superlattices and supercrystals. In lieu of such standard procedures, terms as well-ordered, crystalline order, quasicrystalline, etc. are usually used in literature. However, there exist no commonly accepted definitions of what qualifies e.g. as "well-ordered".

In this review we want to highlight some recent experimental developments and new approaches to study self-assembly of NPs or structure formation of NP supercrystals and their final structure. We focus on NP, the broad field of photonic materials prepared by self-assembly of larger colloidal particles is not covered herein.[8–10] The introduction of the basic concepts of NP self-assembly will be kept short and should be considered as an overview, for more background and details excellent comprehensive reviews are available.[2,11] We will then briefly address and discuss the expectations associated with self-assembled materials, especially the proposed emergence of new properties directly related to order. In the second part of the review, we will present recent innovative approaches for the investigation of self-assembly and self-assembled structures that go beyond the standard characterization. We focus mainly on structure and structure formation and less on properties, so most of the studies are based on scattering and electron-microscopy. **Figure 1** provides an overview roughly following this outline.

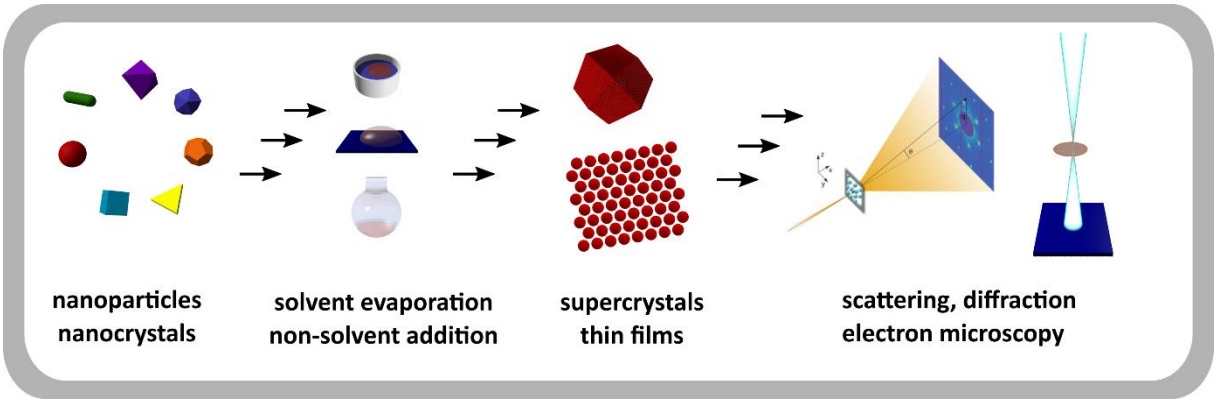

Figure 1. Schematic overview of nanoparticle and nanocrystal self-assembly. In principle the whole range of available nanoparticles with different sizes and shapes and from various materials can be self-assembled. After some purification, concentration and sometimes phase-transfer and ligand-exchange steps, self-assembly can be induced e.g. by solvent evaporation on liquid or solid subphases or by non-solvent addition. The resulting structures range from thin films to bulk-like materials, with all kind of crystal structures and morphologies, ranging from rather disordered structures without defined morphology to well-defined supercrystals with 2D or 3D periodicity. The most important techniques to study self-assembly and the resulting structures are based on electron microscopy, X-ray scattering and diffraction. The organization of the review follows this rough outline.

2 Self-assembly of nanoparticles

Self-assembly is a broad term and occurs on all scales from atoms, ions and molecules to galaxies, as pointed out by Whitesides and Grzybowski.[12] It can be defined as the autonomous organization of multiple discrete components into ordered structures, driven by energetics or entropy or both.[2,13] In nature, countless examples of highly complex and functional structures resulting from self-assembly can be found, for instance proteins and DNA, cells and tissue, chiral liquid crystals with helicoidal organization in some plant tissues, and the cuticles of arthropods[14] or materials with superior properties resulting from biomineralization, e.g. nacre.[15] A key for the understanding of self-assembly is the analysis of involved interaction potentials.[11,16] This can be challenging for nanoparticles because they often can be neither completely described with classical models for larger colloids (d > 100 nm),[17] nor with those describing atomic, ionic, and molecular interactions. In the case of magnetic NPs, magnetic interparticle interactions are involved additionally.[11,18,19] Typically, the self-assembly of nanoparticles aims for a system in thermodynamic equilibrium,

characterized by a minimum of the free energy (or Gibbs free energy), sometimes termed static self-assembly in contrast to the dynamic self-assembly ubiquitous in living systems.[13,20] In the experiment, the formation of dynamically arrested non-equilibrium disordered phases like colloidal glasses and gels or aggregates is to be avoided.[11,21] The interaction potential and length scale of interaction is key in this respect. Too strong attractive short-range interactions result in arrested non-equilibrium states.[11] If attractive short-range interactions (like van der Waals (vdW) forces) are used to induce self-assembly, they have to be sufficiently weak to allow resampling and reorganization of the dense phase towards the thermodynamic minimum. This minimum can often be rationalized with straightforward closest packing arguments.[2] It can be shown for hard spheres (i.e. without attractive interactions and thus no favorable (exothermic) enthalpic contributions to the Gibbs free energy) that maximizing packing density by crystallizing into fcc or hcp (or other stacking variants of hexagonal layers yielding a space filling or volume fraction $\varphi = 0.74$) maximizes the total entropy, because the increased local degrees of freedom for each NP outweigh the reduced configurational degrees of freedom of the ensemble compared to a disordered assembly ($\varphi_{max} \sim 0.64$).[2,22] The other extreme in this respect is the assembly of soft spheres (deformable but incompressible) that is governed by minimization of contact area, favoring e.g. a bcc over a fcc structure. The majority of inorganic NPs can be described as a hard core with a soft organic coating (the ligands),[23] thus in between these extrema, and their self-assembly behavior has to be analyzed accordingly.[24] A comprehensive discussion can be found in the review of Boles et al.[2]

2.1 Ligands for self-assembly

The ligand coating of nanoparticles dictates their interactions with the environment and therefore plays a crucial role in their self-assembly as well.[25] In self-assembly experiments not only the molecular structures of the ligands themselves have to be taken into account, but also their grafting density and organization on the NPs' surface, that can be strongly affected

by the solvent and also by co-solutes.[26–28] An intuitive example is the ionic strength of an aqueous solution, dictated by the salt content, that is directly related to the electrostatic interaction potential of charged particles.[29] Another relevant example is the presence of free ligands, that cannot be avoided for various types of NPs without reducing their colloidal stability.[30] Also the ratio of ligand shell thickness to inorganic core diameter can play an decisive role. Depending on this ratio, the core or the ligands can dominate the interparticle interactions and the structure of the ligand shell can be affected significantly.[31]

Three classes of ligands are typically used for self-assembly: DNA-based, small molecules and polymers.[32] DNA-based ligands, i.e. oligomers, come along with the attractive feature of being "programmable" via base-pairing, enabling the design of complex structures and crystal lattices.[33–39] The drawback of DNA-mediated assembly is the requirement of aqueous buffered solutions, limited stability after drying, and limitations regarding the achievable minimum interparticle spacing in supercrystals and superlattices, that is especially important for strong interparticle coupling. In addition, DNA has intrinsic flexibility. For thermodynamically stable binding at room temperature, several base pairs are needed, and due to the small radius of curvature of NPs, the outer parts of the DNA coating are then not rigid, which complicates the formation of larger supercrystals.[40,41]

In the class of molecular ligands, it is notable that the vast majority of ligands are fatty acids, or structurally related to fatty acids, i.e. containing one or more alkyl chains. Typical examples are oleic acid and oleylamine, trioctylphosphine and trioctylphosphine oxide, and dodecanethiol.[2,32] Many of these originate from the synthesis of small NPs (radii < 8 nm), which readily self-assemble into ordered structures from their nonpolar solvents. Arguably the majority of the literature on NP superlattices and supercrystals is still based on such small NPs with hydrocarbon-ligands.[2,42,43] Large supercrystals with periodicity in 2D as well as 3D have been obtained and various crystal structures could be synthesized including impressive binary structures.[44–47] However, small ligands just stabilize comparably small NPs, their

isolating character is sometimes considered detrimental to some desired properties (e.g. charge transport in quantum dot solids) and the range of accessible gaps is limited. With decreasing size of the inorganic core (d < 2 nm), the regime of clusters is reached. Important differences in comparison to small crystalline nanoparticles are that nanoclusters do not exhibit a continuous band structure but discrete energy levels, and that clusters can be synthesized atomically precise.[48–50] Such clusters crystallize readily and this has been and is frequently used for structure elucidation and to study properties.[1,51,52] These nanoclusters are considered as a class of materials on its own and their crystallization is not in the focus of this review.

The limitations regarding accessible interparticle spacings (gaps) can be overcome by using polymer-based ligands, that allow tuning of interparticle gaps via their molecular weight.[53–55] Various polymers and polymer mixtures have been used, but one prominent and notable example is certainly the functionalization with polystyrene-based ligands in various studies for controlled assembly in solution and self-assembly into 2D and 3D superstructures.[32,56–59] Polymers, in some analogy to NPs, can be considered as a class of materials with endless possibilities to tune and tailor properties via their structure. They offer great potential for the integration of NP superstructures into devices by engineering the chemical, rheological and mechanical properties of nanocomposites. Examples are robust freestanding NP supercrystal films, wafer-scale coatings or nanoelectronic devices, to name a few.[60–64] As they are larger than molecular ligands, polymers can to some extent compensate for limited uniformity and dispersity of the NPs, on the other hand this leaves more configurational space for non-crystalline phases, e.g. somewhat ordered assemblies but with no long-range periodicity. In fact, self-assembled polymer-coated NP superstructures with crystallinities matching those of supercrystals based on small NPs with small hydrocarbon ligands mentioned before are still quite rare. Another important class of polymers are block-copolymers. The study of their self-assembly into various complex structures constitutes an own field of research.[65] In the form

of nanocomposites or by using them as a ligand they can also be used to direct the self-assembly of NPs.[66,67] One convenient method to embed NPs into layered polymer shells is layer-by-layer assembly.[68] In this way the interparticle distance can be tuned by the number of polymer layers.

DNA-based - small molecules - polymers is just a rough classification. Dendritic ligands[69–71] and surfactants like cetyltrimethylammonium bromide or chloride (CTAC and CTAB) are examples that do not perfectly match these categories. For instance, CTAC and CTAB are very important and commonly used ligands in the synthesis of spherical and anisotropic gold NPs in water and can stabilize even large nanostructures (> 100 nm) by forming a surfactant bilayer and providing electrostatic stabilization via their polar trimethylammonium termini. Self-assembly of CTAC-coated nanocrystals has been demonstrated for various sizes and shapes including in combination with soft-lithography for hierarchical structures, which are especially interesting for ultrasensitive surface-enhanced spectroscopies.[72–75] It should be noted however, that many self-assembly strategies with initially CTAC or CTAB coated nanocrystals include ligand exchange, e.g. with oligo- or poly(ethylene glycol)-based ligands, which can improve control, stability and reproducibility,[76–80] and with regard to biological applications also biocompatibility.[29]

2.2 Experimental strategies

In a typical self-assembly experiment, NPs are dissolved in a good solvent, stabilized by their ligand coating, that can provide purely steric stabilization (e.g. hydrophobic coatings in nonpolar solvents), purely electrostatic stabilization, or a combination of both.[81,82] In this colloidally stable dispersion, the interparticle interactions are dominantly repulsive.[2] To induce self-assembly, the interactions can be tuned to become weakly attractive. There are multiple ways to achieve this, but most frequently solvent evaporation or non-solvent addition are used.

Some non-polar NPs exhibit a concentration-dependent colloidal stability, in some analogy to molecular solubility.[83] Evaporation of the solvent inevitably leads to "colloidal supersaturation" of the dispersion, resulting in heterogeneous or homogeneous nucleation of crystalline seeds, which can grow via different routes (e.g. aggregative or diffusive) to larger crystals, completely analogous to atomic, molecular or ionic crystallization. As for these classic crystals, control of the evaporation conditions can be crucial[84] and usually slow evaporation is considered to be favorable for the formation of supercrystals with large domain sizes und few defects.[2,85,86] It should be noted, however, that also very fast (in the range of seconds) self-assembly protocols based on solvent evaporation are reported[60] and supercrystal formation in seconds by high-temperature crystallization[87] or induced by hydrostatic pressure has been observed.[88,89] As discussed above, attractive interparticle interactions are not crucial for self-assembly. Well-ordered entropy-driven assembly is well known for hard-spheres and rods.[11] In fact, for larger colloids attractive interactions are often to be avoided.[85] However, most NPs used for self-assembly are characterized by some attractive ligand-ligand vdW interactions in the absence of a good solvent.

This is also the basis of strategies using non-solvent addition or diffusion, thereby decreasing the quality of the solvent for the NPs in a controlled manner.[2,46] Controlling the gas phase above the solutions can help to improve control and reproducibility of self-assembly experiments based on non-solvent addition or evaporation.[2,46,85] A straightforward experimental strategy for evaporative self-assembly is simply drop-casting the NP dispersion onto the desired substrate. More sophisticated methods include Langmuir-Blodgett techniques,[85] electric or magnetic fields or tailored flows.[90] In addition to the physicochemical properties of the NPs and the solvent, their interactions with the substrate play a key role, dictating wetting behavior and wanted or unwanted adhesion of the NPs.[84] For instance, this can be seen in many transmission electron microscopy (TEM)

characterizations of drop-casted colloidal NPs, in which NPs with low dispersity can assemble into 2D-periodic fragments upon drying of the NP solution on the TEM grid.

Adding to the complexity of the process, substrate effects can increase the difficulty of achieving predictable and reproducible self-assembly, but they can also be used to guide it or fabricate hierarchical structures in template-assisted approaches, by using patterned substrates and/or soft lithographic techniques.[80,85,90–92]

The idea of assembling molecules on a liquid subphase for the preparation of defined layers, invented by Irving Langmuir and Katherine Blodgett in the early 20th century, can be adapted for NP assembly as demonstrated in pioneering studies on water.[93–96] One important advantage of this approach is, that the formed NP superlattice films can be transferred to arbitrary substrates. For instance, the classical Langmuir-Schaefer technique of contacting the film with a hydrophobic substrate and carefully lifting the film from the water surface can be used. If a polydimethylsiloxane (PDMS) stamp is used for contacting, microcontact printing allows further transfer of the supercrystal film to other substrates.[93–95,97] Assembly on water as a liquid subphase is not optimal for all NPs. Therefore, the method was later refined by using ethylene glycol and diethylene glycol instead.[98,99] This method was successfully adapted by Dong *et al.* to prepare large scale binary NP superlattice films.[100]

Sessile droplets are an alternative to a liquid subphase in a through or well and are also frequently used, especially for the preparation of monolayer supercrystals.[2,60,101] In a notable example of a drop-casting approach the authors added a small additional amount of the nonvolatile dodecanethiol ligand to the solvent toluene to tune its evaporation behavior and prevent void formation associated with solvent dewetting.[102] Large crystalline monolayer domains of small gold NPs (AuNP, core d ~ 6 nm) with few defects were obtained. Interestingly, in a later mechanistic study it was found and shown that the self-assembly in this system in fact takes place at the liquid-air interphase, i.e. in analogy to evaporation on an immiscible liquid subphase, probably favoring the large scale crystalline assembly.[103] On the

liquid subphase (or at the liquid-air interface, respectively) the particles and formed islands of small self-assembled superlattice fragments can diffuse freely, which is advantageous for resampling and reorganization to arrive at a thermodynamic minimum instead of dynamically trapped states and for avoiding unwanted pinning effects.[103] The assembly on liquid subphases is mostly used to prepare mono- or few-layer superlattices of NPs,[32,60,86,100,103–109] but it is also possible to obtain thick crystals (> 1 μm thickness) with a layered structure.[110] The approaches discussed briefly here: evaporation on solid and liquid subphases and non-solvent-addition, are probably the most common, but various other experimental approaches to self-assembly exist.[85,111] For example, large icosahedral supercrystals could be obtained by spherical confinement in emulsion droplets,[112] and this emulsion-templated self-assembly approach can be scaled up for certain materials.[113,114] Especially in the context of macroscale device fabrication, 2D and 3D inkjet printing with NP-based inks is a promising technique.[63,115–119] It has been shown recently, that it is possible to combine 3D printing and colloidal (diameters 80-1000 nm)[120] or NP (d = 15 nm)[121] self-assembly to produce millimeter- to centimeter-scale crystalline superstructures. Along the same lines the application of mild pressure and/or heat are promising approaches to obtain stable macroscopic materials self-assembled from NPs.[59,122] For macroscale structures and devices the thermal and mechanical stability is an important concern and receives increasing attention.[62,63,122] Not all types of NPs are available by reproducible, scalable syntheses in high quality today, and the same holds true for supercrystal syntheses. Research in this area is still needed to facilitate transfer of NP-based technologies into devices for the proposed applications. On the other hand, there is ongoing interest in new interesting structures and physical properties from a very fundamental point of view, prioritizing rather well-defined, sophisticated, than large scale structures.[4,123,124] Which structural features and properties are important thus depends on the specific direction of research or desired application, that in turn depends on the NP material.

2.3 Structures obtained by NP self-assembly

The terms NP superlattice, supercrystal or supracrystal are not always consistently used and not rigorously defined. In fact, the International Union of Pure and Applied Chemistry (IUPAC) definition of superlattices refers to superlattices in semiconductor technology, i.e. periodically layered structures with chemically different layers.[125] From a crystallographic point of view, a lattice is a mathematical abstraction to describe the periodicity of a structure,[126] so the terms supercrystal, supracrystal, or superstructure are probably preferable when referring to the materials. A special class is represented by the so-called mesocrystals, an abbreviation for mesoscopically structured crystal.[15,127] Usually this term is used for NP supercrystals where the NPs are single crystals (i.e. nanocrystals) and their atomic lattice has a defined common orientation with respect to the superlattice. The common notation with Miller indices is used to describe the crystal structure. Indices like SL and AL (e.g. $(100)_{SL}$, $(110)_{AL}$ … for planes) indicate whether the superlattices or the atomic lattices are referred to. Typical NP superstructures reported are thin-films with defined thicknesses (e.g. monolayers) over comparably large areas,[128] supercrystals with well-defined facets and crystalline habits/morphologies like octahedra, tetrahedra and twinned and/or truncated versions thereof,[2,47,129] and structures with some extent of intrinsic crystalline order but without well-defined morphologies. For instance, the latter can be rough thin films with many voids and islands or very thick assemblies with irregular morphology. If the NP starting material is available in sufficiently large quantities, as in the case of iron oxide NPs,[130,131] and is stable enough, it can be manipulated by classical material engineering techniques, e.g. pressed into large pellets while maintaining its crystalline order.[122] Order formation upon drying is thermodynamically favored for nearly any NP shapes, so it should be kept in mind that even dried NP films and materials that would not be considered “crystalline” but rather heterogeneous and disordered at first sight, often feature some degree of local, sometimes hidden, order.[132–134] For many shapes, formation of crystalline superstructures can be

thermodynamically even more favorable than for spheres,[135–137] e.g. perovskite nanocrystals with a cubic structure are known to crystallize readily.[111]

The whole range of available NP materials, sizes and shapes can potentially crystallize into self-assembled structures and the ligand chemistry allows for a wide range of interparticle gaps within the superstructures, so the structural diversity and complexity of crystalline superstructures is practically unlimited and the interest in new intriguing structures is ongoing.[44,45,135,136,138] However, for many fundamental studies of structure formation and structure-property relationships seemingly "simple" structures already provide proper challenges for scientists and are a good starting point to explore the class of self-assembled materials.

2.4 Defects and order

It is quite popular to describe NPs in supercrystals as artificial atoms, and in fact there are several analogies that help to understand and describe structure formation and crystalline structure of NP supercrystals. For example many defects in NP supercrystals and also their response to mechanical stress can be described with classical shear theory of crystalline materials.[139] On the other hand it is probably just as instructive to consider the limitations of the atom-NP analogy and to be aware of the *differences* between them. Most importantly, in contrast to atoms, NPs are not monodisperse and also never perfectly uniform. NP dispersity, the involved ligands and the complex interplay of various forces from molecular interactions to fluid dynamics in typical self-assembly experiments give a lot of room for structures which are somehow ordered but definitely not nearly as precise as atomic crystals. To account for this, the term quasicrystalline is often used. Consequently, one aspect of the "quality" of a NP-based superstructure is the "quality" of the building blocks itself. The important parameters are the dispersity (coefficient of variation for the size distribution) and the uniformity, that is harder to quantify depending on the shape. For some samples the purity can also play a role, e.g. syntheses of anisotropic NPs might be characterized by their shape

purity. It is often intuitively assumed that a low dispersity and a high uniformity of NPs favor their self-assembly into well-ordered structures. In reports describing new NP syntheses, the spontaneous self-assembly of the particles is even often mentioned to underline the quality of the particles in a reverse conclusion. Of course, this assumption is perfectly reasonable, but systematic studies addressing this question are rare. A polymer coating for instance can in fact compensate for considerable dispersity und shape deviations of the NPs (**Figure 2**).[140,141]

The periodic order or coherence of the crystal structure, if applicable, is usually quantified in terms of domain sizes of single crystalline domains. The density and kind of defects (point defects, grain boundaries, dislocations, distortions etc.) are mostly discussed qualitatively or exemplarily. An important technical parameter for integration into devices is the scale of the superstructure, especially in the case of thin-films. Various nanostructured materials on a centimeter-scale have been reported,[60] but the vast majority of reported NP supercrystals are still mesoscale, i.e. in the range of micro- to millimeters. This scale of the assemblies should not be confused with the domain size of single crystalline domains. These are usually in the range of some square micrometers at maximum with some exceptions. Many reported thin film NP superstructures, especially with polymer-coated NPs, do not exhibit a crystalline order that allows determining domain sizes.[142]

With scattering methods or based on electron microscopy an estimation of orientational disorder is rather straightforward. Nearest-neighbor or pair (radial) distribution function analysis can yield average positional fluctuations. A spherical distribution function (SDF) was introduced recently, that overcomes some limitations of radial distribution functions and the 2D fast Fourier transform when applied to self-assembled NP monolayers with common features of disorder.[143] From diffraction/scattering data, profile and peak shape analysis – from basic to elaborated – can be performed to deconvolute the different contributions to peak broadening and diffuse scattering.[144] X-ray cross-correlation analysis can provide even more in-depth analysis and quantification of order as will be discussed in a later section.

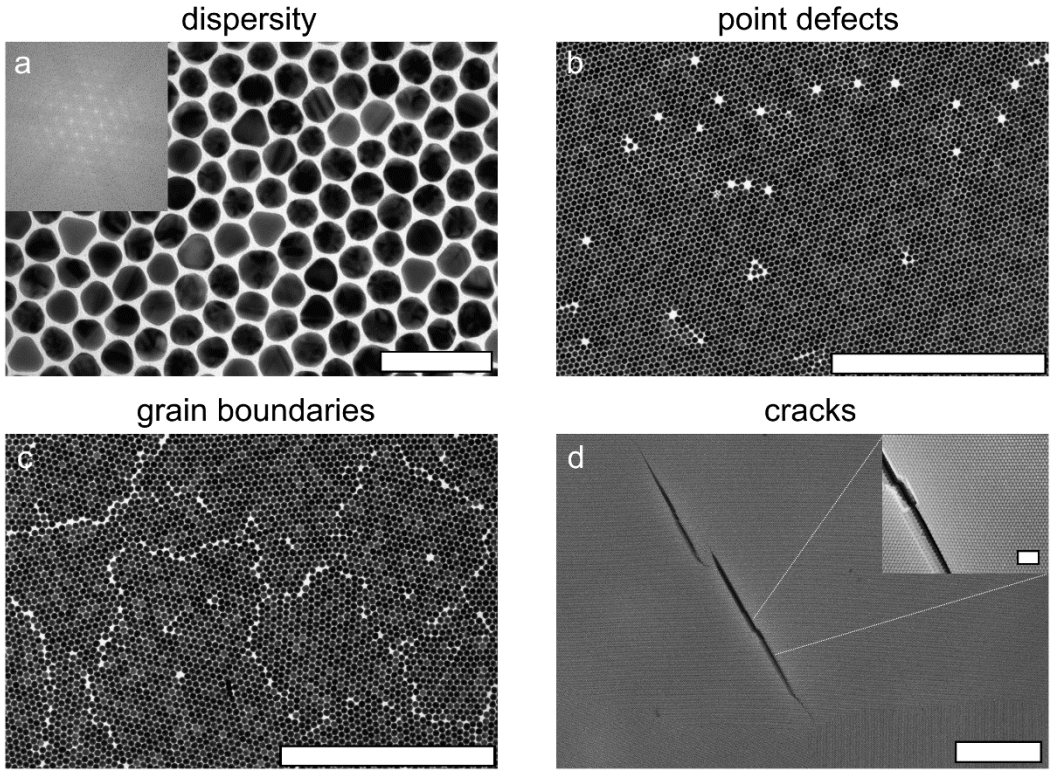

Figure 2. Defects in gold NP supercrystals observed by TEM (a-c) and scanning electron microscopy (SEM) (d). a) despite the dispersity and limited uniformity of the NPs (d_{AuNP} ~ 28 nm, scale bar 100 nm), they arrange in a 2D-hexagonal structure, that can also be appreciated in the fast Fourier transform (FFT) of the digital micrograph (inset). The polymer coating (polystyrene-based ligands with ~2 kDa) might help to compensate for the size and shape dispersity to some extent. b) Point defects (vacancies) in a 2D-hexagonal supercrystal monolayer (d_{AuNP} ~ 50 nm, scale bar 2 µm). c) Grain boundaries in a monolayer (d_{AuNP} ~ 60 nm, scale bar 2 µm). d) Cracks in a hexagonally close packed supercrystal (d_{AuNP} ~ 25 nm, scale bars 2 µm and 200 nm (inset)). Subfigure a) adapted by permission from Ref [140]. Copyright 2018 American Chemical Society and b) and c) by Ref. [57] under CC-BY-NC 4.0.

2.5 What are emerging new properties?

The limited order of NP supercrystals compared to atomic crystals has important consequences. For instance, for the goal of synthesizing quasi-2D quantum solids, i.e. assemblies of strongly coupled semiconductor NPs that allow band-like transport in delocalized hybridized electronic states, as opposed to carrier transport by hopping, energetic disorder is a major hurdle.[6,145,146] Because of the size-quantization effect,[147] energetic disorder is directly related to the dispersity of quantum dots. Additionally, the interparticle coupling depends exponentially on the interparticle separation, thus translational disorder

further contributes to energetic disorder.[145] Even with a size dispersity as low as 3% (about a single atomic bond length) and similarly low translational disorder in a self-assembled monolayer of PbSe nanocrystals the delocalization of the electron wavefunction was still limited to a few unit cells of the superlattice.[146] This example not only illustrates that order and quality of the constituent NPs can play an absolutely crucial role, but also underlines the importance of an accurate structural characterization for a confident analysis and interpretation of structure-related properties. Like the idea of artificial atoms, the possibility of emerging new properties is routinely invoked as a motivational statement in the self-assembly literature. Again, it is worthwhile to reflect: what are emerging new properties? If aggregation is induced in a solution of plasmonic NPs, the optical properties certainly change dramatically in response to structure formation, but at the same time, the changed absorption is certainly not an emerging new property. Likewise, the order and structure of a film of metallic NPs can certainly affect its conductivity significantly,[148,149] and the same holds true for magnetic properties of according NP superstructures,[18,19,150,151] but these are not necessarily new properties. A new property should be more than merely a linear combination of properties of the individual constituents.[61] This brings us back to the analogy with atomic and molecular materials. Ferromagnetism or superconductivity are emerging properties and also the band-transport of electrons in crystalline solids. All of these properties can only be explained with quantum mechanics and are related to strong coupling, extended delocalized electronic states and/or coherent and collective interactions. As discussed, band-like transport in NP supercrystals is hard to achieve, because lack of order, size dispersity and insufficient degree of electronic coupling prevent extended delocalization of electronic states. This can be in part circumvented by coupling dipoles, i.e. electromagnetic fields, instead of electrons, thereby creating collective excitonic or plasmonic states.[57]

For example superfluorescence was recently demonstrated with supercrystals of cubic caesium lead halide ($CsPbX_3$) perovskite NPs (quantum dots).[3] Superfluorescence is a

special case of superradiant emission, the coherent and cooperative spontaneous emission of an ensemble of *N* identical two-level systems with separation distances much smaller than the wavelength of the light field they interact with.[152] If the two-level systems are initially fully uncorrelated, the superradiant emission is termed superfluorescence. In the cubic supercrystals of the $CsPbX_3$ (X = Br or Cl) NPs the photon field established coherence within picoseconds, followed by superfluorescence emission by the correlated excitonic dipoles, characterized by an accelerated photoluminescence decay and longer coherence times.[3] An average number of ~28 coherently coupled quantum dots was conservatively estimated by the authors, who also pointed out that the superfluorescence depends on the assembly and the quality of the quantum dots. Even though the quality was already very high with a size dispersity less than 5% for the quantum dots and monocrystalline cubic supercrystals with lateral sizes up to 5 µm, further improvements of the synthesis might lead to even larger coherently coupled domains. It should also be noted that thermal noise is detrimental to the establishment of coherence and the experiments were performed at cryogenic temperatures (6 K). Very recently also binary and ternary perovskite-type supercrystals were presented underlining the potential of these materials as quantum light sources.[123]

Plasmonic particles like Au NPs have high oscillator strengths allowing plasmonic dipoles to couple to light even more strongly[153–155] and the formation of collective plasmonic states is more tolerant against structural disorder.[156,157] In densely packed supercrystals of large Au NPs (d > 20 nm) light couples strongly to plasmons, resulting in plasmon-polaritons which form standing waves in the supercrystal.[4] In analogy to photonic materials, a plasmonic band structure can be calculated and ultrastrong and deep strong light matter coupling can lead to a polaritonic bandgap, i.e. a range of photon energies where light cannot enter the supercrystal but is reflected (**Figure 3**). Remarkable features of these systems are that deep strong coupling is reached at room temperature and that it can be tuned via the geometry. By changing the molecular weight of the coating polystyrene based ligands, the interparticle gaps

can be tuned[110] and also the core Au NPs with low dispersity (2-4 %) are available in a wide size range.[158] Both parameters affect the coupling strength and the energy of the polaritonic modes. *N*-1 polaritonic modes are possible for *N* layers, so the first mode can be observed for bilayers (Figure 3d). If they can be experimentally realized depends on the quality of the supercrystals,[110] but as mentioned some degree of disorder is tolerated: polaritonic modes were also observed in comparably less ordered systems.[156] As for atomic crystals, different crystal structures of the supercrystals would also lead to different plasmonic band structures.[4] So these materials provide excellent opportunities to manipulate strong light-matter interactions, which is of great interest in the field of cavity quantum electrodynamics[155] but can also be used to tailor surface-enhanced spectroscopies[159] and maybe even hot electron generation for plasmonic photocatalysis.[157,160]

These examples: band-like transport, superfluorescence and deep strong coupling, show that emerging new properties from NPs superstructures are possible and that they naturally depend strongly on the geometry and – to a different extent – on the quality of the supercrystals. An accurate structural characterization is therefore crucial to study and understand these properties but also to even further improve the syntheses of NPs and NP supercrystals. Which defects are important and affect the properties of the material depends on the property. For instance, for the formation of collective plasmonic modes point defects and grain boundaries are quite tolerable but for electric transport they can play a decisive role. Having discussed the "emerging new properties" it is important to point out, that, as fascinating as they are, these are not the only interesting properties that are worthwhile studying and focusing on. Self-assembly should be considered an important and valuable tool, that has and will be applied to successfully create a plethora of new valuable materials for a myriad of applications in various fields as nanomedicine and nanobiotechnology, soft-robotics, optical metamaterials, sensors, materials with tailored mechanical properties and self-healing materials,

nanoelectronics, energy storage and conversion, catalysis, data storage and information processing to name some.[2,19,61–63,72,161–164]

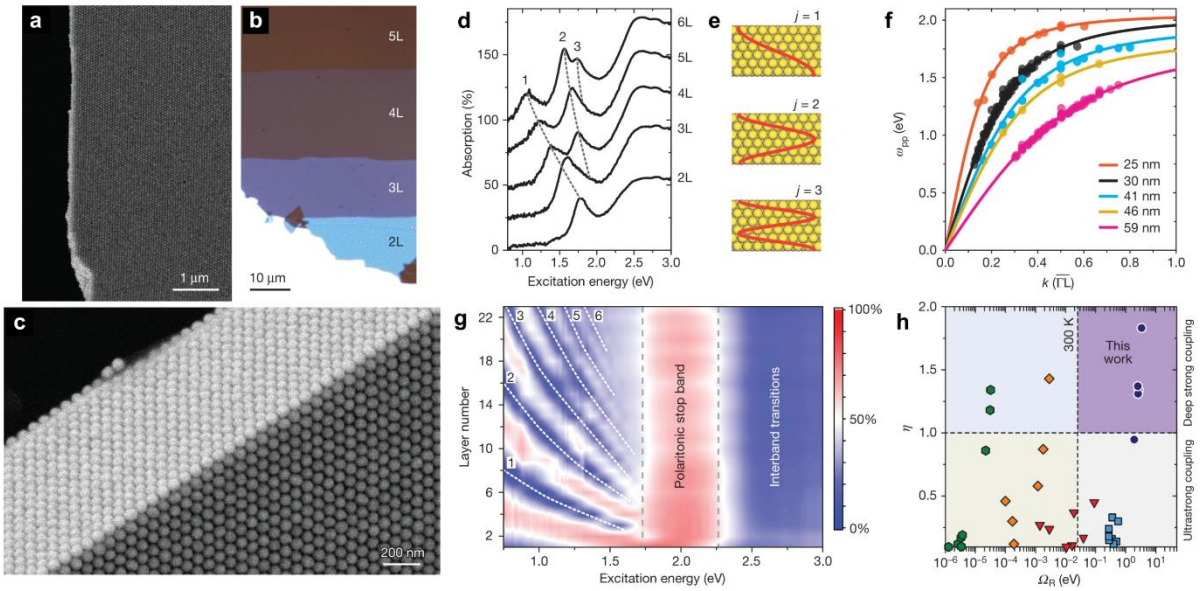

Figure 3. Deep strong coupling in plasmonic supercrystals. Polystyrene coated Au NPs (d_{AuNP} ~ 60 nm) crystallized into defined layered close-packed structures ranging from mono- (**a**), bi- and few- (**b**) to multilayers (**c**)**.** The number of layers can be clearly discerned with optical microscopy in transmission mode (**b**) enabling micro-absorbance-spectroscopy (spot size ~ 1 μm) on defined numbers of layers. Measuring the energies (**d**, shown for d_{AuNP} = 30 nm) of polaritonic modes associated with standing waves in the supercrystals (**e**, j = $2h/\lambda_{PP}$ with the crystal height h and plasmon polariton wavelength λ_{PP}) together with the structural characterization yielding λ_{PP} allows extracting the polariton dispersion. The dispersions for different geometries (d_{AuNP} as indicated and different interparticle spacings (gaps) in the range 1-4 nm) are characteristic for ultrastrong and deep strong light-matter coupling (**f**). Another characteristic feature is the formation of a polaritonic stop band ("band gap") (**g**). The normalized coupling strength ($\eta = \Omega_R/\omega_{Pl}$ with the Rabi frequency Ω_R and the plasmon frequency ω_{Pl}) indicates that light-matter interactions in the supercrystals are in the ultrastrong or deep strong coupling regime at room temperature, depending on the geometry (**h**). Adapted by permission from Ref. [4], Copyright Nature Publishing Group 2020.

3 Characterization of NPs assemblies and supercrystals

The standard characterization methods for NP supercrystals are electron microscopy (EM) and X-ray-scattering/diffraction-based methods, both offering unique strengths and advantages.[144,165] Transmission electron microscopy (TEM) and scanning electron microscopy (SEM) allow real space analysis of local structure with high resolution, the highest resolution being achieved with state-of-the-art TEM allowing under optimum conditions direct imaging of even light atoms as hydrogen and carbon.[166] X-ray scattering and diffraction can probe periodic structures on multiple length scales, also routinely

achieving sub-atomic resolution in X-ray crystallography.[167] The length scale of NPs and NP superstructures is probed by small-angle X-ray scattering (SAXS), but in many studies the orientation of the atomic lattice is also of interest and therefore probed with wide-angle X-ray scattering (WAXS). One difference of SAXS and EM is that SAXS probes comparably large ensembles, thus providing robust statistics, but without resolving individual particles, whereas EM allows for intuitive assessments of particle uniformity and dispersity, their arrangement and defects, but in a small region and with limited statistics.[168,169]

As an example, consider the particles in Figure 2a. Both, SAXS and TEM analysis could provide a measurement of mean particle size and dispersity in good agreement.[169] A SAXS form factor measurement in solution would be statistically much more robust, easily probing millions of particles (depending on particle concentration, beam size and integration time), whereas a TEM analysis usually covers just several hundreds of particles. Similar considerations hold true for the crystalline structure over large scales and in volume materials. On the other hand, the shape dispersity (deviations from sphericity) of this sample or defects as in Figure 2b could hardly be recognized in SAXS data. Thus, the methods are somehow complementary and it is highly recommendable to use both for the characterization of NP superstructures whenever possible. The development and steady improvement of modern synchrotrons as sources of partially or fully coherent X-rays with high intensity provides excellent opportunities for the study of NP supercrystals and their formation. In the recent years the number of studies using such sources has increased considerably and we will discuss them in detail in a subsequent section. For electron microscopy, notable developments are in situ liquid-phase TEM and tomography approaches, which we will cover briefly. For interested readers comprehensive topical reviews are available.[170–181]

3.1 Electron microscopy

With aberration-corrected electron optics not only the spatial resolution of TEM has been significantly improved to picometers but also the energy resolution (~100 mV).[182] The

imaging modes of TEM include high-resolution TEM (HR-TEM), scanning TEM (STEM), and 3D electron tomography.[183] Spectroscopy modes provide element specificity. These include energy-dispersive X-ray spectroscopy (EDX) electron energy-loss spectroscopy (EELS), and cathodoluminescence spectroscopy (TEM-CL). Electron diffraction can be utilized with selected area electron diffraction (SAED), convergent beam electron diffraction (CBED), and nanobeam electron diffraction (NBED). Thus, with TEM it is possible to analyze nanomaterials with atomic resolution and element-specific. The combination of STEM and EDX is commonly used to obtain elemental maps. The scattering of electrons by atoms depends strongly on their atomic number *Z* and this is used in high-angular annular darkfield STEM (HAADF-STEM) to provide elemental contrast with high resolution.[184,185] HR-TEM providing atomic resolution is an invaluable tool for materials science, however in the case of NP supercrystals one is more interested in the arrangement of the NPs than that of the atoms. Even if the orientation of the atomic lattices is of interest, as in the case of perovskite and other quantum dot superstructures, the ensemble level is more relevant, i.e. if and how well the crystalline NPs are commonly oriented within the supercrystal. Of course, TEM can be and is used with low magnifications to provide overviews of the supercrystal structure, but then (in contrast to diffraction/scattering) the resolution is inevitably diminished. TEM is limited to thin film samples, depending on the material ~100 nm thickness can already prevent meaningful analysis. SEM has a lower resolution than TEM (typically in the range 1-20 nm)[165] but allows to image the surfaces of thick samples because it is not a transmission technique but measures secondary and back-scattered electrons. As for TEM, spectroscopic information like EELS, EDX and CL can be obtained for elemental analysis. Therefore, SEM is an excellent tool for large-scale overviews of supercrystals, thick samples (which can be tilted during the measurements) and 3D structures like the polyhedral morphology of supercrystals.[2,186] SEM is also advantageous in terms of scale in electron tomography.[187] Electron tomography in TEM is usually based on HAADF-STEM[172,173,173]

and limited to assembly sizes of about 500 nm.[187] By combining focused ion beam (FIB) and SEM, tomography on significantly larger scales is possible.[187,188] In this approach a focused beam of gallium ions is used for precise consecutive milling of thin (~ 3 nm) slices of the sample, combined with SEM imaging. It was demonstrated recently, that with this approach individual nanorods could be resolved in larger superstructures than with electron tomography based on TEM, and in very large volumes colloids could be individually resolved where it was not possible with confocal microscopy.[187] This approach therefore bridges the gap between TEM and light-based microscopy. In another recent study a supercrystal block (V = 8 μm^3), part of a larger structure assembled from gold octahedra (edge length 75 nm) in a microfluidic device, was reconstructed in 3D with FIB-SEM tomography confirming the local hexagonal order throughout the crystal.[72]

It should be noted that, despite the limited accessible volume, TEM electron tomography can be extremely powerful.[170–173,189,190] With improved reconstruction algorithms it was demonstrated that icosahedral assemblies of Fe–Co–O NPs (d ~ 9 nm) could be reconstructed in 3D on a single particle level for structures up to 300 nm in diameter, containing nearly 10,000 particles.[189] In a recent study a similar analysis was demonstrated with binary (CdSe NPs with d = 7.7 nm and PbS NPs with d = 9.9 nm both d including the ligand coatings) icosahedral assemblies.[191] Modern instruments offer temperature control in a wide range and this was used in a recent study to study thermal structure-switching of supercrystals of Au NPs (core d = 4.1 nm) with HAADF-STEM and complementary in situ and ex situ electron microscopy and small-angle XRD.[192] To allow for the thermoresponsive crystallinity of the superstructures, the Au NPs were functionalized with a liquid-crystal-like ligand. A bct phase was observed up to 80 °C that underwent a phase transition to a bcc phase at higher temperatures and another phase transition above 130 °C into a fcc phase that was stable up to 215 °C. The phase transitions were reversible with a low temperature hysteresis and repeated switching between the bct and bcc phase was possible. Based on a thorough structural

characterization, the authors found that by optimizing the number of thermal annealing cycles and the cooling rate the crystalline domain sizes could be increased significantly.

Another notable development is the use of pixelated detectors (electron microscope pixel array detector, EMPAD), allowing so-called 4D-STEM, where 2D images (real space or diffraction) are collected over a 2D-grid of the scanning probe positions.[193,194] This was used to combine STEM and NBED to elucidate superlattice transformations of PbS cuboctahedron (~ 7 nm) NPs monolayers with single nanocrystal resolution. Specifically, the precise position and atomic lattice (AL) orientation (in plane and out of plane) of nearly all ~300 NPs in the field of view could be deduced.[195] Based on the data the authors could show that the assembly and transformation of PbS NP monolayers on ethylene glycol proceeds via a pre-aligned ($<11n>_{AL} \parallel <11>_{SL}$) hexatic into the final square lattice in which the alignment AL-SL is further optimized. The transformation was induced by injecting ethylene diamine into the liquid subphase. The assembly behavior can be understood considering the facet-specific binding behavior of the oleic acid ligands, which are known to play a key role in the assembly, transformation and oriented attachment of these type of NPs (PbX, X = S, Se).[196–199] With the rapid development of detector technology it can be expected that 4D-STEM modes including user-friendly data processing and analysis solutions will be integrated in commercial instruments in the near future and become more and more accessible and available.[194] This provides excellent opportunities for the studies on self-assembled materials, e.g. when the atomic-lattice orientation is crucial.

3.2 Liquid-phase TEM

TEM in the liquid phase (LP-TEM) is technically challenging, because the use of solvents is intrinsically incompatible with the required ultra-high vacuum in the instrument. In principle it is possible to use solvents with negligible vapor pressure like ionic liquids or molten salts but the more common approach is the use of tightly sealed sample cells with electron-transparent silicium nitride (SiN) windows enclosing a thin film of the liquid (< 1 µm).[181]

Within the last two decades a lot of progress has been made in the design and fabrication of such sample chambers and commercial solutions are available today. Flow-cells, temperature control, included electrodes, user friendly dual-chip cells and more have been implemented and with modern microfabrication techniques the reproducibility and control of the geometry and the stability of the closed-cells has improved significantly.[174,176,200] Graphene is in principle superior to SiN as a window material in terms of minimum thickness and stability and used for innovative cell designs[201,202] but graphene based cells are also more challenging to handle.[174,179] Liquid-phase SEM (LP-SEM) approaches[203] as well as spectroscopy modes[204] are also possible and similar considerations hold true as for ex situ EM, namely that the resolution of LP-SEM (4-10 nm) is lower than that of LP-TEM but larger structures can be measured. A detailed discussion of the different technical approaches and their specific advantages can be found in a recent progress report.[174]

The challenges in LP-TEM studies include control and measurement of the effective liquid film thickness[205] and managing beam and substrate effects. The input of significant doses of high energy electrons induces solvent radiolysis, strongly affecting the ionic strength, and can cause heating, charging effects and convective flows.[177,206] Together with the substrate interactions of significant proportions of the sample in the thin films, the Brownian motion of NPs is strongly affected. In fact, unhindered Brownian motion of particles in LP-TEM has only recently been observed experimentally at high viscosities and/or low electron flux.[206,207] It has to be taken into account carefully when interpreting LP-TEM measurements, that they might not be representative for bulk conditions. Because of the presence of solvent in the beam path the contrast is decreased compared to dried samples and using low electron doses to minimize beam induced effects further decreases the signal-to-noise ratio.[177] Despite all these challenges, the prospect of monitoring NP assembly in real-space and real-time is very attractive. Many LP-TEM studies addressing self-assembly do not use the term as it is used herein. Instead of describing the formation of comparably large superstructures with some

extent of crystalline order, often rather the assembly of dimers, small clusters and chains of NP is studied focusing on dynamics and pairwise interactions.[174,179,208–212]

Self-assembly into larger structures with some local order was studied e.g. by Lee et al.[213] The authors focused on the effect of solvent drying, comparable to the final stage of drop-cast induced evaporative assembly. They found that the solvent boundary plays a decisive role by transporting particles by lateral dragging and flattening aggregates by vertical pressing. Which of these factors was dominant depended on the NP concentration. Another study monitored the assembly of small (d ~ 4 nm) dodecanethiol-coated AuNP.[214] Based on image analysis of LP-TEM measurements, the authors calculated the contributions of Brownian motion, vdW-interactions, steric hindrance and hydrodynamic drag forces. They found that the cluster growth kinetics can be reasonably modeled by reaction-limited Brownian aggregation. In the initial phase of self-assembly the Brownian forces dominated, whereas in the late stage of assembly short-range vdW forces within the formed clusters became equally important. The delicate balance of the multiple short-range attractive vdW and repulsive steric interactions resulted in a dynamical nature of the formed clusters, which exhibited some degree of hexagonal order.

An interesting example of radiolysis induced self-assembly was studied by the Chen group. They functionalized gold nanoprisms (edge length ~ 90 nm, thickness 7.5 nm) with small amphiphilic thiol ligands with terminal carboxylic acid groups, yielding particles which are at least in part electrostatically stabilized. In aqueous buffer solutions (0.15 M PBS, pH 8) all carboxylic acid groups are deprotonated and the prisms assemble face-to-face into columns with interstices between nearest-neighbor-prisms dictated by the balance of vdW attraction and electrostatic repulsion.[215] Because electron-beam-induced radiolysis changes the ionic strength significantly, the electrostatic repulsion and therefore interstices are also affected and the d-spacing (nearest-neighbor-distance of the stacked prisms) could be related to the dose rate and ionic strength of the solution and therefore be used for calibration in the low dose

range. At higher doses (> ~ 6 $e^-/(Å^2 \cdot s)$) the *d*-spacing was constant until at high doses (> ~ 1000 $e^-/(Å^2 \cdot s)$) representative for conventional TEM and most LP-TEM studies the prisms coalesced. In a subsequent study with similar prisms (edge length ~ 100 nm, thickness 7.5 nm) an interesting hierarchical superstructure was found, formed by organization of the stacked columns into a hexagonal arrangement (**Figure 4**).[216] Assembly and melting of the superstructure could be triggered by simply switching the beam on and off, proving that electron-induced radiolysis modulated the ionic strength and thereby the electrostatic interactions. Using particle tracking and Monte Carlo (MC) simulations it was shown that the positional order of the columns originates from the orientational disorder of the prisms within the columns resulting in isotropic intercolumn interactions. Also, the squared modulus bond orientational order parameter $\left|\psi_{6j}\right|^2$ (to quantify the sixfold symmetry) and the local density (inverse of the according Voronoi cell) for each column during the crystallization process was computed. This way, a two-step nonclassical crystallization pathway could be deduced in which a metastable intermediate dense liquid-like phase formed from which crystalline domains nucleated and grew. Such studies demonstrate how real-space and real-time single-particle tracking analysis of LP-TEM data can contribute to our understanding of self-assembly of nanocrystals and nanoscopic phase-transitions of soft matter in general.[177,178,217]

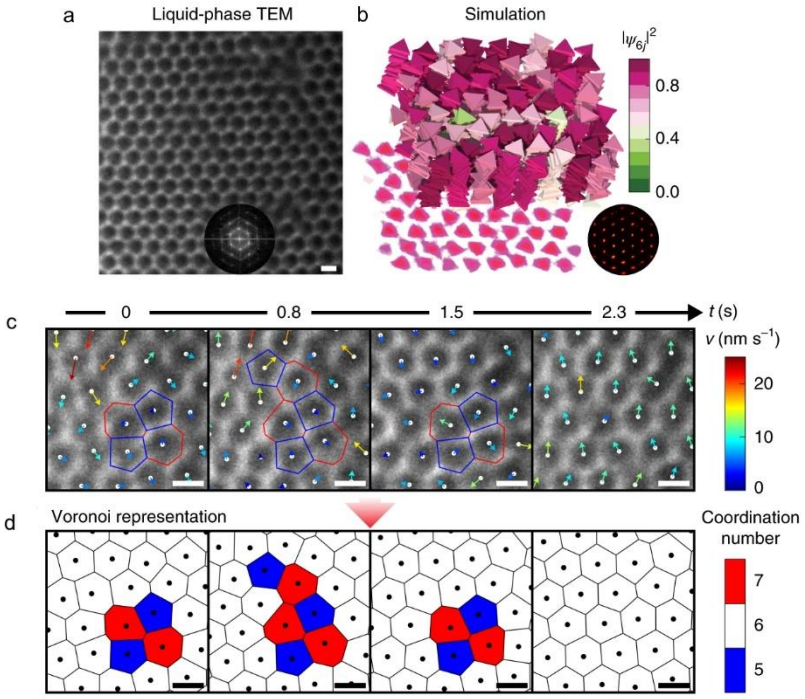

Figure 4. Hexagonal superstructure of columns of stacked gold nanoprisms. **a**) LP-TEM of the hexagonal superstructure, the inset shows the FFT of the image. **b**) MC simulations confirming that the hexagonal superstructure is thermodynamically favored. The color code denotes the squared modulus of the bond orientational order parameter $|\psi_{6j}|^2$ per column j. The 2D projection of the superstructure and the diffraction pattern further illustrate the hexagonal order. **c**) Time-lapsed LP-TEM images and d) corresponding Voronoi representations showing the annealing of imperfectly coordinated sites. The coordination number of each cell is indicated by the color code. Arrows in c are colored by the magnitude of the instantaneous velocity of individual columns v calculated from successive LP-TEM images. Scale bars for all images: 100 nm. Adapted by permission from Ref. [216], Copyright Nature Publishing Group 2020.

4 X-ray scattering methods

4.1 Small Angle X-ray Scattering (SAXS)

In scattering experiments on bulk samples, the modulus of the wave vector transfer

$$|\mathbf{q}| \equiv q = \frac{4\pi}{\lambda}\sin\left(\frac{\theta}{2}\right) \quad (1)$$

has to match the length scale to be probed via $d \sim \frac{2\pi}{q}$. In order to study structures of nanoscale materials of $d \approx 1$ to 100 nm, typical wave vector transfers are thus in range of 10^{-2} to 1 nm^{-1}. With hard X-rays as probe ($\lambda \sim 1$ Å) this leads to small scattering angles below $\theta = 1°$. Therefore, this technique is called small-angle X-ray scattering (SAXS). In contrast, X-ray diffraction (XRD) at large angles covering atomic resolutions is referred to as wide-angle X-

ray Scattering (WAXS). The small angles are typically detected by using large sample-detector distances of several meters. In extreme cases, ultra-small angles are measured at USAXS instruments with sample-detector distances up to 30 m,[218] that allow detection of structures beyond 1 µm. Nowadays, SAXS is a standard setup for structure determination of nanoscale materials,[144,219] and many different experimental approaches use this geometry, e.g., X-ray Photon Correlation Spectroscopy for investigating sample dynamics[220,221] or tomography approaches for revealing hierarchical structures.[222] SAXS experiments cover many research fields such as, e.g., soft matter characterization,[223,224] biological macromolecules,[225] structure of NPs,[144], compressibility of liquid water[226] and many more.

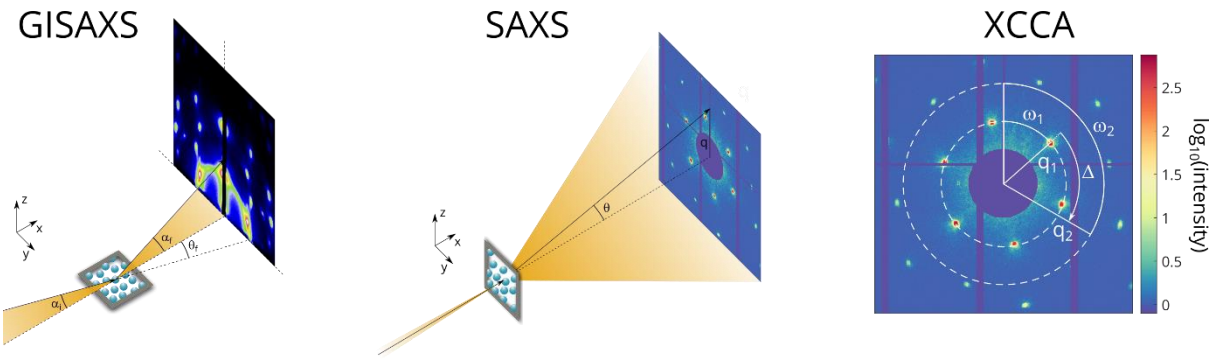

Figure 5. Schematic settings of GISAXS and SAXS, as well as definitions of XCCA. The GISAXS pattern is taken from Weidman et al.[227], the SAXS pattern is reproduced from Schulz et al.[228] under CC-BY-NC 4.0.

A basic geometry of a SAXS experiment is shown in **Figure 5**. The X-ray beam impinges on the sample and the scattered intensity is measured in forward direction by a two-dimensional detector. In this geometry, the intensity is given by the Fourier transform of the electron density of the probed volume. In the single particle limit, e.g., dilute colloidal dispersions, $I(q)$ measures the form factor of the particles

$$F(\mathbf{q}) = \frac{1}{V_P}\int_{V_P} \exp(i\mathbf{q}\cdot\mathbf{r})\, dV_P \qquad (2)$$

via

$$I(\mathbf{q}) = \delta\rho^2 V_P^2 |F(\mathbf{q})|^2 \quad (3)$$

Here, V_P is the volume of one particle and $\Delta\rho$ the density difference between particle and solvent. In practice, many samples, especially in solution, have an isotropic shape or are measured as average over all orientations. Therefore, the azimuthally averaged intensity $I(q) = \langle I(q,\omega)\rangle_\omega$ is typically subject of the experiment.

At higher particle density, the scattering signal is additionally affected by the inter-particle structure and one obtains $I(q) \propto |F(q)|^2 \cdot S(q)$. The static structure factor $S(q)$ is given by the Fourier transform of the pair distribution function $g(r)$. Depending on the state or phase of the sample, the shape of $S(q)$ differs, e.g, one observes Bragg peaks for crystalline materials or a broad peak around $q_0 \approx \frac{2\pi}{d_0}$, with the next-neighbor distance d_0, and an oscillating behavior around 1 for liquids and amorphous matter.

SAXS is performed using laboratory X-ray sources as well as at synchrotron radiation sources. The latter provide a significantly higher X-ray flux, which allows larger flexibility of beam sizes and geometries. In particular, millisecond time-resolutions are nowadays standard for in situ and in-operando studies at many sources. A flexible X-ray energy allows furthermore the usage of complicated sample environments such as high-pressure cells[229–231] where the X-rays have to penetrate diamond windows demanding a high flux at high X-ray energies. Besides, SAXS allows precise measurement of particles sizes, shapes and size distributions providing complementary information to EM methods. For instance, using Monte Carlo methods[232,233] different populations of gold nanoparticles have recently been measured,[168] and the size evolution of nanoparticles can be tracked in in-situ experiments.[234]

4.2 Grazing-Incidence Small-Angle X-ray Scattering (GISAXS)

In SAXS experiments, an ensemble average of the bulk structure is probed with an incident beam perpendicular to the sample surface. In order to study structure and structure formation

at surfaces and interfaces, a grazing-incidence geometry is used. As for X-rays the index of refraction is slightly below 1 with $n \approx 1 - \delta$ and $\delta \approx 10^{-7}$ to 10^{-5} depending on the wavelength and material properties, external total reflection is found for incidence angles below the critical angle of $\alpha_c \approx \sqrt{2\delta}$. In GISAXS experiments, the X-ray beam hits the sample surface under a small angle, typically slightly below or above α_c. In this way, the penetration depth of X-rays can be tuned, typically from below 1 nm up to several 100 nm and thus the surface-sensitivity can be adjusted.[235,236]

The GISAXS geometry is shown in Figure 5. Similar to SAXS experiments, the scattered intensity is measured on a 2D detector several meters downstream the sample. At shorter detector distances, one usually refers to grazing-incidence diffraction (GID) as analogue to XRD probing atomic and molecular length scales. Due to the symmetry-breaking of the surface, the scattering pattern is usually anisotropic and shows contributions from surface scattering. Thus, the scattering vector is analyzed in the $q_y - q_z$ plane, which are defined as:

$$q_y = \frac{2\pi}{\lambda}[\sin(\theta_f)\cos(\alpha_f)] \quad (4)$$

$$q_z = \frac{2\pi}{\lambda}[\sin(\alpha_f) + \sin(\alpha_i)] \quad (5)$$

For $\theta_f = 0$ and $\alpha_i = \alpha_f$ the intensity only reflects the specular scattering with $q_y = 0$. This method is known as X-ray reflectometry, which can quantify structures perpendicular to the surface in the sub-nm range.[235,237] The so-called out-of-plane components with $q_y \neq 0$ give rise to the structure parallel to the surface, the depth information is given by q_z. Furthermore, as for the low incident angles the beam footprint on the sample is rather large, in the range of cm, GISAXS provides an ensemble averaged surface or interface structure. Therefore, GISAXS is frequently used to study surface processes, such as nucleation and growth of islands and films and particularly allows one to identify the shape of grown islands. GISAXS has become a standard technique at synchrotron radiation sources as well. In general, the

same characteristics apply as for SAXS, such as the possibility of probing in situ with (sub-)millisecond time resolution.

4.3 X-ray Cross Correlation Analysis (XCCA)

In a typical SAXS experiment as discussed above, a one-dimensional scattering information is probed. In this way one obtains average information about the structure of a sample, e.g., by the static structure factor $S(q)$. However, in particular during order formation in, e.g., phase transitions, such average information is not enough to quantify structural differences. This is demonstrated in **Figure 6**. The higher degree of order visible in the two-dimensional scattering pattern may be lost by averaging, and the so-obtained structure factor resembles the one from a liquid state. XCCA, sometimes also denoted as fluctuation X-ray scattering (FXS), is one way to access such orientational order information via angular correlations from two-dimensional scattering patterns, as highlighted in Figure 5. The use of two-dimensional spatial correlations from X-ray scattering has been introduced in the 1970s to obtain reconstructions from single particle structures.[238] However, the low intensity of laboratory sources prevented its application on those times for X-rays, while the concepts have been used in the 1980s in laser scattering experiments.[239] With the availability of modern synchrotron radiation and Free-electron laser (FEL) sources, application of XCCA has been shown experimentally during the last decade.[240–243] Currently, XCCA techniques are one of the routes for single particle imaging at FEL sources, e.g., for studying virus particles.[244]

In parallel to the reconstruction studies, XCCA has been demonstrated to provide valuable information beyond pair correlations in condensed matter. In the first study by Wochner et al.,[245] the authors found evidence for a five-fold local ordering in colloidal hard-sphere glasses. In the following, theory works showed the potentials and limitations of this method.[133,246–251] Besides studies on NP self-assembly, XCCA was applied in different X-ray scattering experiments on, e.g., symmetry of magnetic domains,[252] ordering in liquid crystals,[253–255] polymers[256,257] and colloids,[258] particle orientations and structures in liquid

jets[259–261] as well as correlations between dynamics and structure close to vitrification of hard spheres.[262]

In XCCA experiments, the local order is obtained from the full two-dimensional scattering pattern. Thereby, correlations of scattered intensity are calculated between different points on the scattering pattern. Here, we limit ourselves to two points on the scattering pattern $I(\mathbf{q}) = I(q,\omega)$ for clarity, a more general approach is given in a topical review.[263] Typically, correlation functions

$$C(\mathbf{q_1},\mathbf{q_2}) = C(q_1,q_2,\Delta) = \frac{\langle I(q_1,\omega)I(q_2,\omega+\Delta)\rangle_\omega - \langle I(q_1,\omega)\rangle_\omega \langle I(q_2,\omega)\rangle_\omega}{\langle I(q_1,\omega)\rangle_\omega \langle I(q_2,\omega)\rangle_\omega} \quad (6)$$

are calculated in XCCA experiments. This parameter peaks if the intensities $I(q_1,\omega_1)$ and $I(q_2,\omega_2)$ with $\Delta = |\omega_2 - \omega_1|$ are correlated. The average is calculated over all azimuth angles ω. For many applications, intensities are correlated at the same q, i.e., $q_1 = q_2$. In this case, the equation becomes

$$C(q,\Delta) = \frac{\langle I(q,\omega)I(q,\omega+\Delta)\rangle_\omega - \langle I(q,\omega)\rangle_\omega^2}{\langle I(q_1,\omega)\rangle_\omega^2} \quad (7)$$

In order to quantify the local order, Fourier coefficients $\hat{C}_\ell$ of C with respect to Δ are investigated. It can be shown, that C_ℓ can be expressed by the Fourier coefficient of the normalized intensity $I^N(q,\omega) = \frac{I(q,\omega)-I(q)}{I(q)}$, with the average intensity $I(q) = \langle I(q,\omega)\rangle_\omega$, as $\hat{C}_\ell(q) = \left|\hat{I}_\ell^N(q)\right|^2$. Besides the amplitude of local order thus given by the modulus of $\hat{I}_\ell$, the orientation of the particular symmetry can be obtained by the phase Ω_ℓ of the Fourier coefficients

$$\hat{I}_\ell(q) = \left|\hat{I}_\ell(q)\right| \exp(i\Omega_\ell(q)) \quad (8)$$

Then, the orientation angle of the ℓth symmetry is given by $\theta_\ell = \frac{\Omega_\ell}{\ell}$.

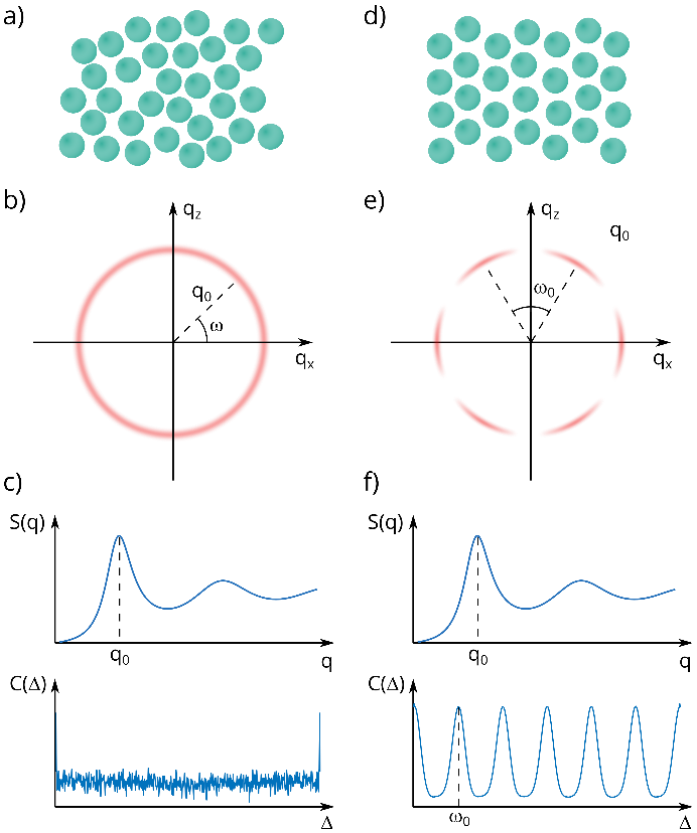

Figure 6. X-ray scattering from amorphous (**a-c**) and crystalline (**d-f**) structures. An amorphous sample (**a**) gives rise to a diffuse scattering signal with a broad ring at q_0 corresponding to the next-neighbour distance d_{nn} by $q \sim \frac{2\pi}{d_{nn}}$ (**b**). Azimuthal integration yields the structure factor $S(q)$, the cross-correlation function does not show any hint for local ordering (**c**). In contrast, the scattering signal from an ordered assembly (**d**) shows distinct peaks (**e**). However, by integration this information is lost and a $S(q)$ similar to the amorphous sample may be obtained. Nevertheless, the order is reflected in peaks in C that resemble the six-fold symmetry of the sample (**f**).

4.4 Assembled structures probed by XCCA

Recently, XCCA has been applied in a rising number of studies. Besides gaining insights into the lattice type,[264] XCCA has been particularly used to obtain information on the assembled domains and correlation between crystalline NP and superlattice structure.

Domain characterization using XCCA

The application of XCCA in combination with SAXS was demonstrated to provide information on domains of similar order. Schroer et al. introduced a combination of X-ray microscopy and XCCA for structure determination of thin films.[265] A film of a mixture of dried silica NPs with radii of 11 and 19 nm was studied by a 400 nm small X-ray beam. The film was scanned vertically and horizontally by steps matching the beam size. As scattering

methods provide the structure averaged over the illuminated volume, the spatial resolution is defined by both the beam size and the scan step size, i.e., about half a µm in this case. The composition and thickness of the film is subsequently obtained by the intensity measured at corresponding q values that show either strong scattering from the small or the large particles. This microscopy approach was extended by an additional cross correlation analysis from each scattering pattern. In this way, intensity maps of the sample were compared to the local order map obtained from XCCA. Furthermore, the phase Ω_ℓ of the 4th and 6th Fourier coefficients was used to obtain the orientation of ordered domains, reporting domain sizes of few µm. Such spatial maps of orientational order have also been used for liquid crystals to study hexatic-smectic transitions.[266,267]

This technique has been extended for self-assembled films of Au NP with 100 nm to 700 nm thickness.[132] The films consisted of 27 nm Au NP that have been functionalized with poly(ethylene glycol) (PEG) ligands of about 10 nm length. Using as well a 400 nm sized beam, few 1000 particles were exposed at each measured spot. Typically, regions of 30 µm x 30 µm have been investigated, yielding about 3600 scattering patterns which corresponds to experimental scanning time of about 1 h. The authors found heterogeneous structure with dominating 4- and 6-fold symmetry. Comparing spatial maps of I_4 and I_6, strong sixfold order resulted in weak fourfold order and vice versa. Most interestingly, a symmetry-dependent domain size of 3.5 µm for sixfold order and approximately 1.2 µm for fourfold order was found. In a follow-up study, the authors reported a dependence of the local orientational order of the assembled films on the ligand composition.[134] Moreover, the addition of salt further reduced the order of the films due to screening of the charged particles during the assembly, suggesting a complex symmetry-selective assembly process.

The strength of cross-correlation analysis combined with TEM was recently demonstrated in a study on plasmonic supercrystals.[228] These were polystyrene coated Au NP with a very low size dispersity of about 4% at a core diameter of 24 nm. As mentioned in an earlier section

and shown in Figure 3, using these AuNP, large areas of many 1000 µm^2 of well-defined thickness ranging from mono-, bi-, tri- to multilayers can be obtained. The exceptional plasmonic properties of these systems strongly depend on their geometry,[4,110] requiring decent structural characterization. Here, TEM was used to investigate the structure of selected regions of interest, resolving single particle properties. The same regions could be studied by the scanning SAXS-XCCA approach, revealing domains of maximum size, i.e., single domains were filling whole mesh areas on the TEM grids. As a combined approach, the structure of the supercrystals can be studied over many length scales ranging from single particles with sub-nm resolution by TEM up to millimeters and beyond using X-ray scattering. Results of this study are shown in **Figure 7**. While TEM allows to identify layer thicknesses and structure up to at most four or five layers, this restriction does not exist for the scattering approach. With the SAXS-XCCA analysis an increase of the lattice constant as a function of number of layers was found while the high degree of orientational order was constant. Statistically robust measurements of such sub-nanometer structural features and quantitative evaluation of crystalline order would not be possible with TEM alone.

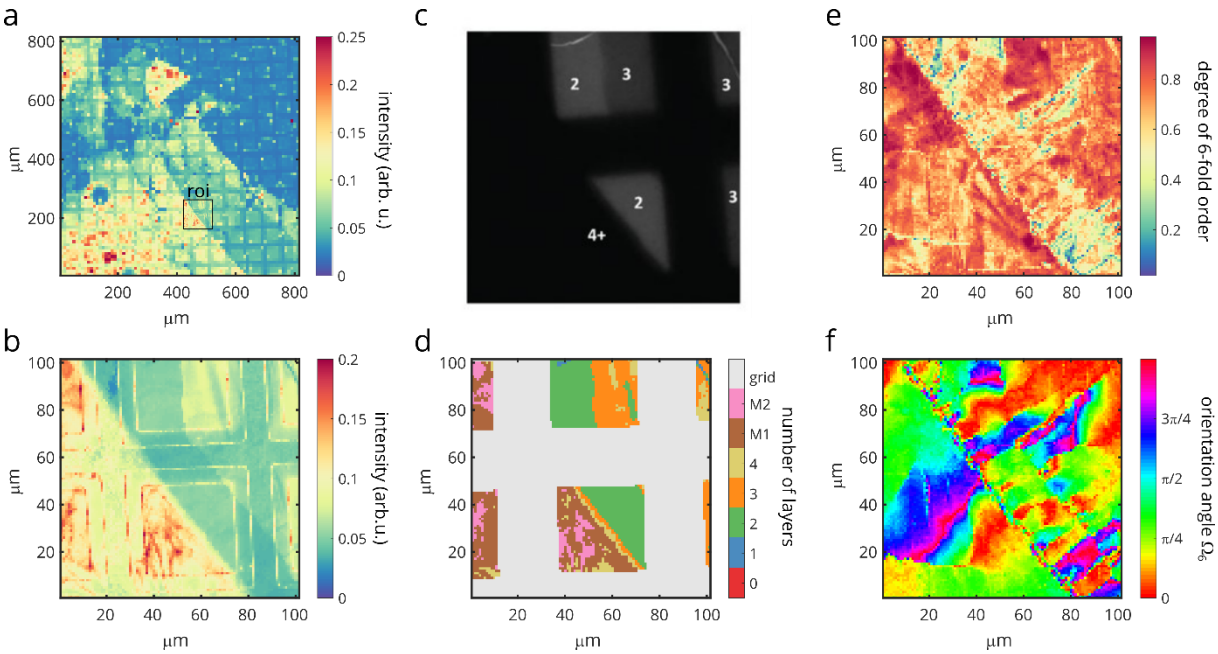

Figure 7. Combined TEM-SAXS-XCCA approach for structural studies of plasmonic films.[110] (**a**) Intensity map covering 800 µm x 800 µm shows the overall morphology of the sample. The underlying TEM grid is clearly visible. (**b**) Intensity map of the region of interest

(roi) marked in (**a**) studied with 1-µm step size. (**c**) TEM image of the same roi allows identifying layer thicknesses up to three layers. (**d**) Layer thicknesses as measured from the scattered intensity in the SAXS experiment can be assigned up to multilayers (M1 and M2). (**e**) High degree of sixfold order I_6 for the same roi. (f) Orientation angle Ω_6 showing large domain sizes close to 1000 µm^2. Other rois showed domains filling the whole TEM mesh. Figure is reproduced from Ref.[110] under CC-BY-NC 4.0.

Nanoparticle-superlattice correlations

A particular strength of XCCA has been shown in several studies on assemblies of PbS NPs. Zaluzhnyy et al. studied assemblies of PbS NP with a diameter of about 6.2 nm.[266] These quantum dots typically exhibit polyhedral shapes resulting in truncated octahedral, cuboctahedral or cubic shapes. Consequently, their self-assembly into supercrystals might be driven by the orientation of the particles. In the experiment, scattering from single grains was analyzed using as well a nanofocused X-ray beam. Utilizing a large 2D detector at a short sample-detector distance of about 40 cm, a q-range of 0.7 nm^{-1} to above 22 nm^{-1} could be covered in the experiment. This enabled synchronous measurement of the supercrystal peaks that are found in the SAXS regime at low q values below 2 nm^{-1} and the Bragg reflections originating from the atomic lattice in the WAXS regime at q values above 16 nm^{-1}. The supercrystal was identified to exhibit a distorted body-centered cubic (bcc) arrangement known as body-centered tetragonal (bct) structure as found in other studies of similar particles.[227,268] The atomic lattice is of Fm3m type, of which the {111} and {200} reflections could be measured. Due to the simultaneous measurements of all these Bragg reflections, the angular correlation of the supercrystal and the atomic lattice could be calculated. In this way, the orientation of the NPs with respect to the superlattice was determined. The authors found a strong correlation between the atomic lattice and the supercrystal. This was further specified obtaining two different configurations from such q_1-q_2-correlations for PbS NPs with diameter of 6.8 nm,[269] see **Figure 8**. A rotation of all NPs by 45° around the [100] direction of the atomic lattice of the NPs transposes both configurations. Boundaries between domains are characterized by an out-of-plane rotation of the superlattice and the NPs preserving their

angular correlation. This might be connected to stress during the assembly process which resulted in a 5–10% compression of the lattice constant in the grain boundaries.

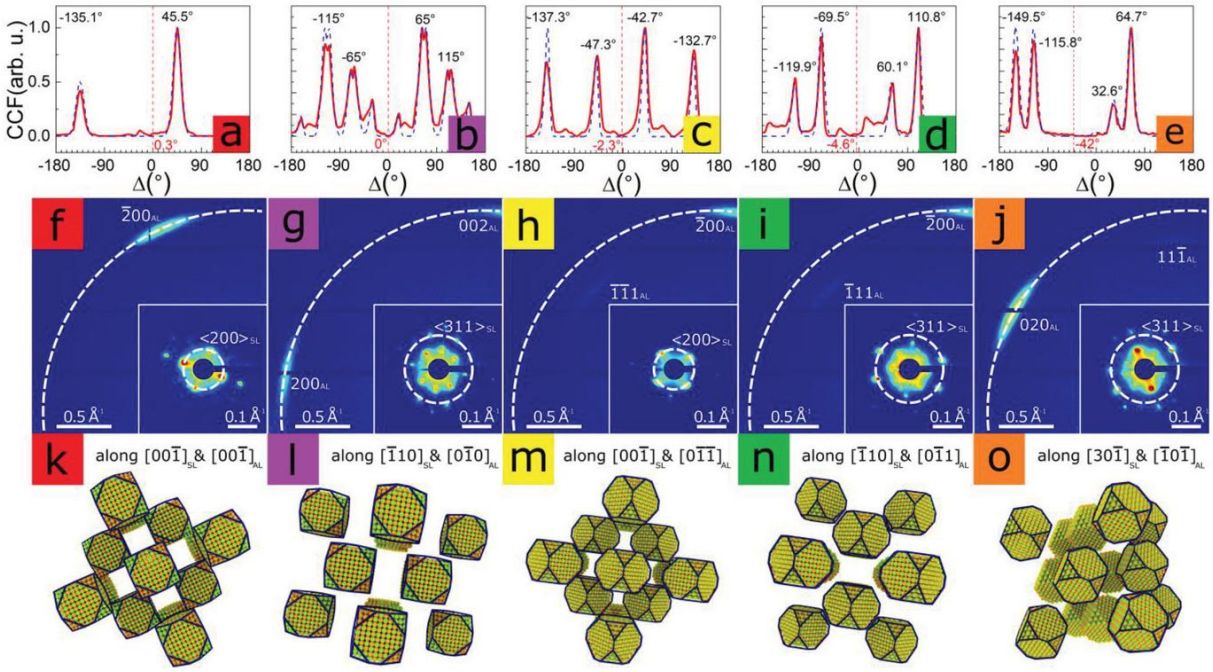

Figure 8. a–e) Experimental cross-correlation functions (CCF, red lines) from five domains together with simulated CCFs (blue dashed lines) based on the model structures shown in (k–o). f–j) WAXS diffraction patterns of each domain. Enlarged SAXS patterns are shown in the lower right corners. The *q*-values used for calculating CCFs are indicated by the white dashed lines. k–o) Real-space models of the superlattice and its constituting NPs based on the SAXS and WAXS patterns and CCFs for all five domains. The red and purple domains represent one configuration, the yellow, green and orange domains represent the second configuration. Reprinted from Ref.[269] under CC BY-NC-ND 4.0.

These methods have been recently used to measure correlation of structure and function. In particular, the direction-dependent charge carrier transport in PbS NP supercrystals has been quantified.[270] To this end, the XCCA results have been correlated with the electronic properties of the same domains. The authors found a clear impact of supercrystal crystallinity on the electric conductivity. An anisotropic charge transport in highly ordered domains was found indicating that transport anisotropy may be common in weakly coupled NP supercrystals.

4.5 In situ studies

The high flux at current synchrotron radiation sources combined with modern two-dimensional detectors enables time-resolved experiments with resolutions down to (sub-)ms.

This matches self-assembly time scales in many cases. In particular assemblies prepared by solvent evaporation taking place on time scales of seconds to minutes can be perfectly probed this way. Consequently, a rising number of in situ X-ray scattering studies on supercrystal formation have been performed in recent years.

The first in situ study of NP self-assembly into supercrystals by SAXS has been published in 1998.[271] Therein the authors studied the assembly of dodecanethiol-stabilized Ag NPs (d = 6.7 nm) with a resolution of 1 s. The NPs formed a fcc superlattice and the lattice constant decreased by almost 1 nm during the assembly process. In the following years, in situ SAXS and GISAXS have become a standard tool for probing the kinetics of NP assemblies. The vast majority of in situ studies using X-ray scattering focus on the assembly of a few classes of NPs, namely iron oxides, gold, and semiconductor materials such as PbS and PbSe. An overview of self-assembly studies is given in **Table 1**. In the following we will review some recent examples, distinguishing between surface and bulk studies.

Table 1: X-ray scattering studies probing the in situ assembly or structural changes of different NP materials.

NP material	Method	References
Iron oxides	SAXS	[272–279]
	GISAXS	[280,281]
Au	SAXS	[88,89,282–289]
	GISAXS	[290,291]
PbSe	SAXS	[292]
	GISAXS	[293–296]
PbS	SAXS	[297–299]
	GISAXS	[109,199,227,296,300–302]
CdSe / CdS	SAXS	[303]
	GISAXS	[304]
Ag	SAXS	[271,305]
Pd	SAXS	[87]

Self-assembly at interfaces

The majority of in situ studies is performed at interfaces. Here, GISAXS is the method of choice, providing structural information at and close to the interface with high spatial resolution normal to the interface. A recent review focuses particularly on quantum dot self-assembly probed by GISAXS,[236] so the discussion here is restricted to some recent highlights.

Time-resolved GISAXS studies have particularly benefited from the development of fast detectors, reaching sub-millisecond time scales.[306] In an early demonstration, this enabled studying assemblies in drying liquid drops where a critical drop size was found that is necessary for the assembly of iron oxide NPs.[280] In the following, particular interest was spent on studying the assemblies of quantum dots, such as PbS,[109,227,300,301] and PbSe[293–295] with GISAXS, but also iron oxide NPs[281] and semiconductor nanorods.[304] While the studies focused on different aspects and driving forces of the assembly, e.g., the role of the ligands,[109,296,301] many of them reported a two-step assembly process. As an example, we want to discuss this in more detail based on the study presented by Weidman et al. in 2016.[227] Using faceted 5.6 nm PbS NPs shaped as a truncated octahedron capped with oleic acid, the authors showed that these NPs form a bcc lattice with a lattice constant of about 9 nm as measured from the final dry assembly. The kinetics of the assembly was studied by GISAXS and GID from an evaporating droplet of the PbS NPs dispersed in toluene on a substrate. The sample chamber was slowly flushed by helium which let the solvent evaporate over approximately 30 minutes. After about 12 min superlattice formation sets in and it could be associated to a fcc structure. In the following, the structure transferred to bcc, reaching the dried state after 30 min. This transition was linked to the Bain distortion observed in martensite steels. Here, the c-axis contracts whereas the a- and b-axes expand, leading to a transition from fcc to bcc via body-centered tetragonal (bct) intermediates, see **Figure** . Furthermore, from the GID data the authors could further specify the orientation of the NPs, reporting a full alignment already at early stages of the assembly. In a later study the role of

nanocrystal dispersity, ligands and solvent was studied in detail.[307] Therein, the supercrystals were prepared by spin-coating. A strong effect of dispersity was found. Even a moderate increase of the dispersity from 3% to 5% led to significantly decreased grain sizes and strongly reduced alignment of the atomic lattices. The same observation was made for a decreasing ligand coverage (grafting density). Solvent effects were also found, which could not be explained with the different evaporation rates alone, indicating that solvent-ligand interactions also play a decisive role. The best results were obtained with toluene. Aliphatic hydrocarbons (hexane, octane and decane) yielded smaller grains and less alignment. Considering such complex dependencies and additional relevant parameters (preparation method, shape etc.) it comes as no surprise that with similar NPs different structures have been reported. We will discuss this in more detail in the next section.

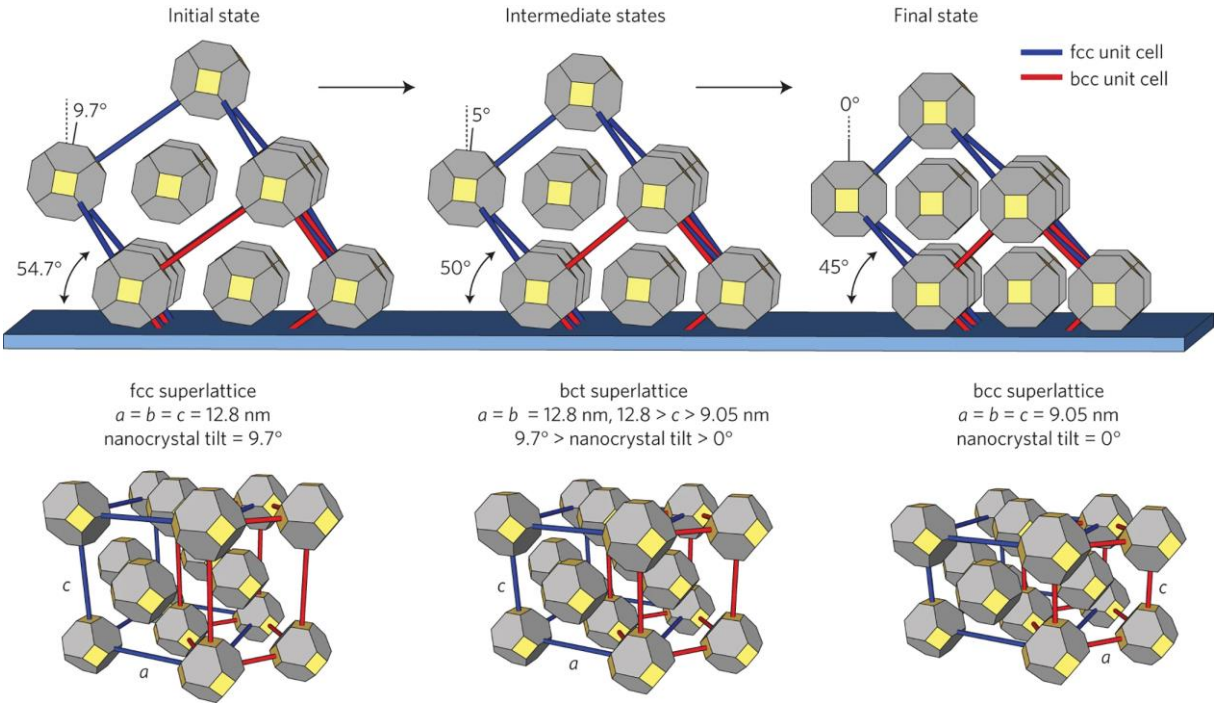

Figure 9. Different structures found during the assembly of PbS NPs at interfaces. Reprinted by permission from Ref.[227] Copyright Nature Publishing Group 2016.

Besides the self-assembly process, technical applications demand a large-scale fabrication of quantum dot films. Such an approach has been recently demonstrated by printing of PbS NPs.[302] This process was studied in detail by in situ GISAXS.[308] The printed films were

found to dry within 30 s in a two-step formation process as well. First, the assembled films form a fcc structure. This is based on an intrinsic templating effect, where the first layer corresponds to the (111) plane of an fcc lattice. Similar to Weidman et al.[227] the structure transfers to bcc in the final stage. In addition, stacking faults are found, resulting in a bcc nested fcc stacking during the assembly.

Evaporative self-assembly from bulk suspensions

SAXS is particularly used in studies on superlattice formation in the bulk. In this section we review recent results on size- and shape-dependence in the assembly of quantum dots complementing the GISAXS studies presented above. Furthermore, SAXS enables the use of special sample environments, such as free-standing or levitating droplets, and provides structural information during changes of solvent properties, temperature or pressure. Instead of studying the formation of PbS supercrystals at the liquid-air interface, Lokteva et al. used a vertical geometry for transmission SAXS.[297] This allowed for monitoring of the superlattice formation and transformation at different stages of the assembly process in real time while the evaporation front moves (**Figure 10**). The evaporation speed can be finely tuned by changing the gas flow around the chamber. The NPs form assemblies on silicon nitride membranes on two sides of the sample cell. In contrast to GISAXS experiments, a full bulk sensitivity is obtained. In addition, the authors combined the SAXS analysis with time-resolved XCCA, reporting a two-step assembly process.[268] A NP size-dependence on the assembly outcome was found as well.[309]

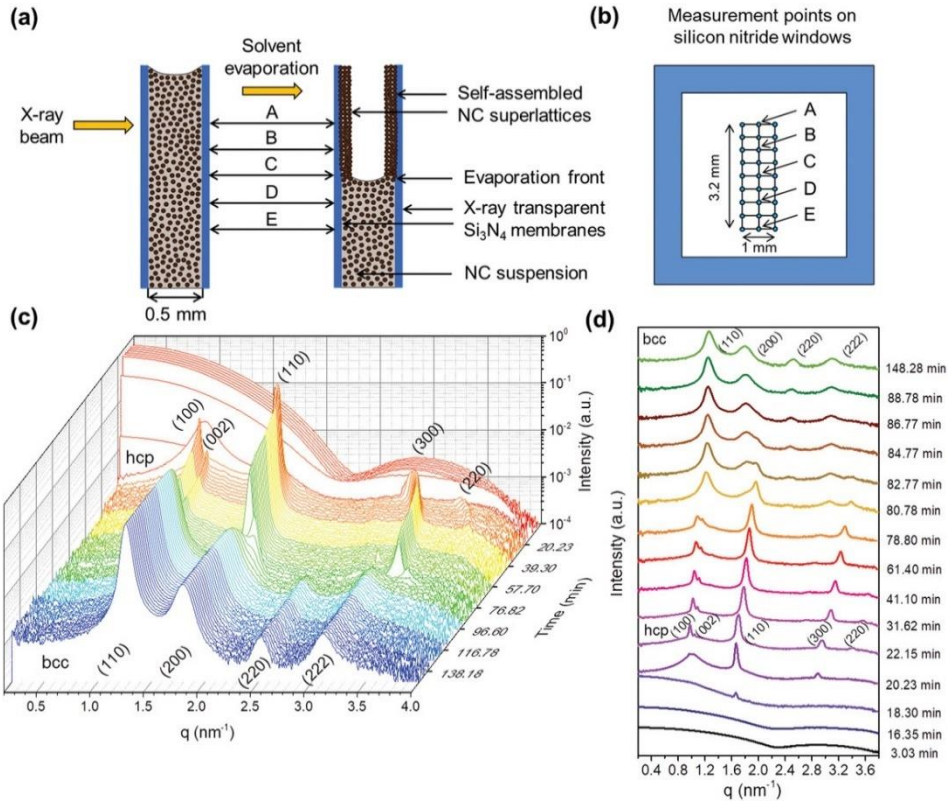

Figure 10. In-situ SAXS experiment on PbS self-assembly. a) Illustration of the sample cell where colloidal PbS NPs (here termed nanocrystals: NCs) self-organize along cell windows upon controlled solvent evaporation. b) Scheme of the measurement points on the silicon nitride windows; points A, B, C, D, and E shown in (b) are depicted as well in (a). c) Time-resolved SAXS curves of PbS NCs in heptane recorded every 2 min at point A. d) 2D representation of selected SAXS curves from (c) for better visualization of the crystal structure evolution. From Ref. [268]

With 4 nm PbS NPs capped with oleic acid ligands, the NPs formed a hcp lattice first, and transformed into bcc afterwards. The hcp lattice was formed at the drying front, at a packing fraction of about 40%. In the following the lattice got gradually compressed up to 60% volume faction and then suddenly changed to bcc. This change happened simultaneously in the whole assembled film, potentially when the residual solvent molecules have been evaporated from the films. Thus, solvent molecules present in the swollen self-assembled superlattices evaporated fast when the chamber became not saturated by solvent vapor anymore, which led to a rearrangement of the crystal structure. A more complex process was observed for 7.8 nm PbS NPs with a cuboctahedral shape.[309] The Bragg reflections of different assembly structures overlap, but their symmetries obtained by XCCA are different.

Using the 2nd, 4th and 6th Fourier coefficients of the cross-correlation function, an hcp structure was observed first, followed by a partial transition to bcc and afterwards to bct. Remarkably, the coexistence of hcp and bct phases was found at the same volume fractions predicted for hard particles of the same shape,[310] suggesting that the shape of the core is preserved with dried ligands.

This raises the question of what defines the structures during and after the assembly process. Comparing these studies with other PbS NP self-assembly results,[227,266,269,301] the NP sizes are slightly different. Therefore, the shapes are likely different as well, and so are the softness values (ratio of the fully extended ligand length to the core radius) and, more intriguingly, the ligand densities, which have an impact on the assembly process and outcome as discussed above. The GISAXS studies used incidence angles below the critical reflection angle of PbS,[109,227,301] so that the structure is only probed in the first few nm. In contrast, the transmission studies[266,268,269,309] provide the average structure of the whole film which may be different from the surface. More studies of the self-assembling behavior are necessary, systematically controlling all parameters of the NPs and the assembly conditions.

This was further highlighted by an in situ SAXS study on the assembly of Fe_3O_4 nanocubes.[273] Different superlattices were obtained, including bcc, fcc, simple cubic (sc) and obtuse rhombohedral (rh) polymorphs in 3D, as well as two-dimensional lattices. Therein, fcc and bcc assemblies were preferred at the early stage, while confinement effects led to transformation to rh distortions. In contrast, sc-type superlattices needed a particular driving force. The authors could establish a consistent phase diagram of the formed superlattices based on reconstruction of the assembly pathways. This demonstrates that such assembly studies are crucial for a controlled design and fabrication of functional materials with desired properties driven by a tailor-made superlattice structure.

Assemblies from evaporating droplets

Like in GISAXS studies, in the majority of SAXS studies the assembly typically starts at an interface, e.g., at a wall of a sample chamber. To avoid such a heterogeneous nucleation process with external materials, Agthe et al. studied the assembly of oleic acid-capped γ-Fe_2O_3 truncated nanocubes in levitating droplets dispersed in toluene (**Figure 11**).[274]

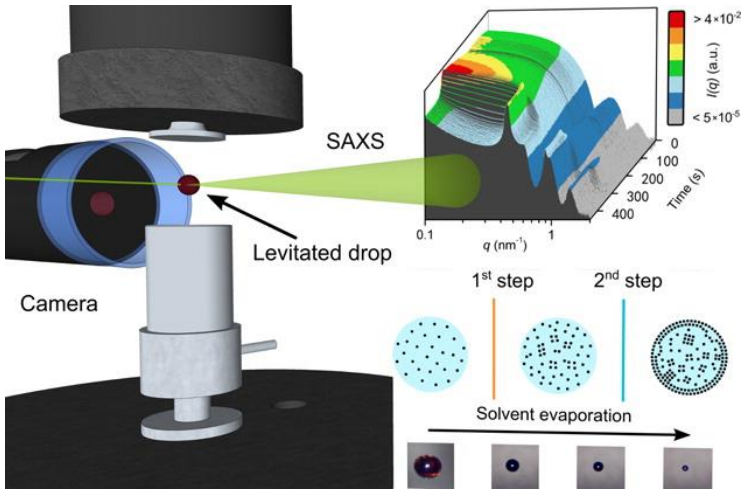

Figure 11. SAXS experiment on levitating droplets. The droplet is tracked in situ by a camera (left). Its radius shrinks with time due to evaporation of solvent (bottom right). This leads to the formation of NP films starting on the droplet surface that gives rise to Bragg reflections in the SAXS curves (top right). Reprinted with permission from Ref. [274]. Copyright 2016 American Chemical Society.

Within few 100 s the toluene evaporated, leaving a dry hollow capsule of assembled NPs. The assembly was found to be mainly diffusion-controlled,[275] leading to a two-step assembly process. First, the NPs form disordered clusters in the bulk. Afterwards, ordered domains are achieved close to the droplet surface when a higher volume fraction is reached. As no container wall is present in such experiments, details about strain evolution were studied as well, revealing that contraction during the superlattice growth is responsible for isotropic strain and the appearance of point defects. In combination with a magnetic field, mesocrystalline fibers built from magnetite nanocubes have been achieved.[279] Before the fibers grew, driven by the magnetic field, micrometer-sized mesocrystals with a cubic shape were formed. The transition from the three- to one-dimensional growth could be connected to the size and field dependence of interactions between the interacting mesocrystals.

Besides such iron oxide nanocubes, in situ SAXS studies on evaporating droplets have been recently used for many different sample systems, including proteins[311] and cellulose nanocrystals,[312] as well as the formation of free-standing two-dimensional assemblies.[313] Wang et al. studied the assembly of polystyrene spheres dispersed in water and found transitions from fcc over random hexagonal close-packed to random close packed structures.[314] They concluded that the self-assembly from evaporating droplets is influenced by both thermodynamic and kinetic effects, including diffusion, convection, and sedimentation of the particles.

Instead of using levitating droplets, Doblas et al. studied the assembly of Au NP from hanging droplets.[83] Millimeter-sized droplets of different NP dispersions hanging at the orifice of a silica tube evaporated within several 100 s. Self-assembly started at concentrations that significantly depended on the solvent. Furthermore, the agglomerates grew, but the concentration of the dispersed, free particles remained at a constant level. The authors found that the colloidal stability was different for different solvents, best in cyclohexane and worst in toluene, suggesting that molecular interactions between solvent and ligand shell play the major role.

Those studies dealt with an evaporating droplet in a gaseous environment. A different approach was introduced recently, studying the assembly of core-shell NPs in an oil-in-water emulsion.[112] This enables the formation of larger supraparticles, i.e., an assembly of NPs forming three-dimensional supracrystals of different shapes, in particular with icosahedral symmetry. The NPs are dispersed in an apolar solvent such as cyclohexane that is later emulsified into water assisted by surfactants and stabilizers. Upon evaporation of the cyclohexane, the effective volume fraction of the NPs increases and finally a supraparticle is formed. This process was later studied using in situ SAXS.[276] During the evaporation of the cyclohexane, a slow increase of volume fraction was observed. At a certain critical volume fraction – 20% in the case of the studied core-shell NPs with FeO core, a $CoFe_2O_4$ shell, and

oleate capping ligands – the assembly suddenly sets in. Using an USAXS setup, the authors could track the size of the oil droplets in parallel to the assembly, showing a rapid shrinkage when the crystallization sets in.

A similar approach was followed by Kraus and co-workers. They reported the assembly of superparticles from gold NP stabilized by alkanethiol and dispersed in oil-in-water emulsions.[315] Using in-situ SAXS, the supercrystals' structure is governed by the liquid-liquid interface and the interparticle potential that resembled Lennard-Jones potentials. Instead of agglomerating quickly, the particles have enough time to find energetically favored positions. As a result, clusters containing "magic" numbers of particles are formed predominantly. In a follow-up study on binary particles with radii of 4 nm and 8 nm, respectively, the authors found formation of AB13 superlattices.[316] Most interestingly, the assembly outcome could be varied by rising the hydrostatic pressure moderately in the range of few bar, resulting in Janus-type supercrystals or core-shell arrangements, i.e., different types of demixing of large and small particles. This observation was confirmed by MD simulations and resembles the demixing of binary alloys with different phase diagrams.

Changing solvent properties

The in situ studies addressed so far were based on the evaporation of the solvent. In this way the effective volume fraction of the NPs increases, until the formation of a superlattice is energetically preferred. The destabilization or modification of the solvent is another route to induce assembly.[2,111] Here, a few time-resolved SAXS studies have recently been performed. The effect of non-solvents on the superlattice formation was addressed by Lee et al. studying PbS nanocrystals stabilized with oleic acid dispersed in toluene.[298] Different polar non-solvents, such as methanol and isopropanol, were added on top of the NP dispersion leading to destabilization of the NP due to interdiffusion of the solvents thereby triggering the formation of superlattices. It was found that the relative miscibility of the ligands, solvent, and non-solvent defines the resulting superlattice structure. Depending on the size and shape of

the NP, different assembly routes have been found as in the evaporation studies. For small NPs (d = 4.14 nm) the SAXS data indicated a fcc-bcc transformation, whereas slightly larger NPs (d = 5.60 nm) showed only an fcc structure during the assembly process. This data was accompanied by small-angle neutron scattering data providing access to the swelling behavior of the ligands. Methanol favors swelling of the ligand shell by toluene, whereas isopropanol extracts toluene molecules out of the ligand shell.

A similar approach was used by Yang et al. studying the assembly of supercrystals from gold nanocubes.[283] The authors deposited a surfactant solution of highly concentrated cetyltrimethylammonium chloride (CTAC) micelles on top of a droplet of the gold nanocube dispersion. The CTAC micelles instantaneously diffuse across the interface resulting in a broadened interfacial region with a gradient of surfactant concentration. The NPs were found to concentrate in this interfacial region leading to a diffusion-driven assembly. Afterwards, the nuclei sediment and grow into supercrystals of µm size within few hours, tracked by SAXS. Lv et al. used a multi-method approach to investigate the superlattice formation by poor-solvent enrichment, modifying solvent composition, initial nanocrystal concentration, poor-solvent enrichment rate, and excess surfactants.[277] In situ SAXS experiments were performed using different solvent modification on evaporating droplets, as introduced in the previous subsection. It was found that a higher crystalline quality of superlattices is achieved with a sufficient addition of excess oleic acid as surfactant which resulted in large and well-ordered supercrystals.

Temperature-induced assemblies

A special case of NP nucleation followed by an immediate assembly has been reported for Pd nanocrystals.[87] Pd NPs were synthesized at temperatures above 230 °C by thermal decomposition of a Pd–trioctylphosphine complex in the presence of hexanoic acid. Directly afterwards, fcc superlattices are formed by the NPs within few seconds. As mentioned earlier, this is remarkable because usually the formation of well-defined supercrystals is assumed to

require more time. Furthermore, the individual NPs grew continuously within the superlattices allowing for fine nanocrystal size control. The authors found that this crystallization process is dependent on both the size of Pd nanocrystals and the type of surface ligands used during the assembly. For instance, different ligand composition during the nucleation may result in hcp structures rather than fcc, or may lead to dissolution of the superlattices at higher temperatures.

Besides nucleation and growth of superlattices, temperature increase may lead to structural changes of the superlattices. Temperature-dependent SAXS studies on dodecanethiol-capped AuNP of 1.8 nm diameter revealed the existence of multiple different structures.[284] At room temperature, the NPs formed a bcc superlattice that transferred to hcp at 125 °C, with a significantly increased next-neighbor distance. Further heating resulted in icosahedral AB_{13} structures around 167 °C, changing again to a hexagonal structure at 177 °C, and a more compact hexagonal superlattice at 181 °C with AB_5 structure. Eventually the superlattice decomposes into domains of coalesced Au and hydrocarbons at high temperatures. Recently, Kim et al. studied the structure of superlattices of poly(ethylene glycol)- (PEG-) functionalized Au NP.[285] The crystalline quality could be controlled via the electrolyte concentration, pH, and temperature of the suspensions. In particular, the interparticle attraction increased with rising temperature up 70 °C, which improved the quality of the supercrystal structure. The lattice constant changed reversibly with temperature and decreased with increasing temperature. This behavior can be understood considering the lower critical solution temperature (LCST) of PEG-water mixtures, the effect of salts (electrolytes) on the solubility[317,318] and that the LCST of PEG and consequently also PEG-coated Au NP can be significantly lowered by salt addition.[319]

A reverse temperature behavior was reported for the assembly of DNA coated gold particles.[286] By cooling from above 50 °C, an fcc superlattice formed with a crystallization temperature depending on the length of DNA linker. The quality of the superlattices increased

further with decreasing temperature. The authors concluded that the superlattice forms via a 3-step process: first the appearance of disordered DNA-Au NP aggregates, followed by localized reorganization and finally growth of crystalline domains. Again this behavior can be understood considering the ligand coating, namely the well-known thermodynamics of oligonucleotide base pairing, double-strand formation and melting.[320]

Pressure-induced assemblies

A new approach to trigger NP self-assembly was reported by Li et al.[303] and Schroer et al.[88] using high pressure for initiation of the assembly. Whereas the interesting effects of pressure on NPs itself and on preformed assemblies have been studied a lot,[321] it is rarely used to induce the assembly. Because for such high-pressure experiments dedicated sample environments with diamond windows have to be used,[229–231] X-rays are excellently suited to penetrate such high-pressure cells, whereas many other characterization techniques can hardly be applied for in situ studies. Li et al. followed the formation of nanowires by oriented attachment and coalescence from CdSe NPs at pressures above 10 kbar.[303] Schroer et al. found that PEGylated Au NP form high-quality fcc supercrystals at high pressures when salt is added to the suspension.[88] Supercrystals were found for NaCl, KCl, RbCl, and CsCl, differing slightly in the transition pressure. Depending on the amount of salt, the transition pressure could be reduced down to 2.7 kbar for 2 mol/l RbCl. Other factors, such as the original Au NP volume fraction in the dispersion or the length of the PEG ligands only played a minor role. The latter, however, dictated the interparticle spacing within the supercrystals and led to different compressibilities. Without salt, the interaction of these NPs was found to change from repulsive to attractive at high pressures due to a collapse of the PEG ligand shell,[322,323] however, no supercrystal formation was found up to 4 kbar pressure.

This was further investigated in time-resolved experiments after a pressure jump.[89] Therein, the pressure was raised from below to above the crystallization pressure within few milliseconds. The subsequent supercrystal formation and growth was tracked by time-

resolved SAXS. In general, the supercrystals form rapidly within seconds and faster. Furthermore, the faster the NP superlattice forms, which basically depends on the width of the pressure jumps, the better the crystal quality. These results are in line with a rapid change of the solvency of the PEG ligand in the aqueous solvent. When the critical pressure is reached, the solubility of the PEGylated Au NP is reduced and water is expelled from the PEG shell, suggesting the existence of a lower critical solution pressure. This route demonstrates the formation of high-quality superlattice at very short times. However, after pressure release the superlattice melts, so that fixation methods would be needed at such high pressures for superlattice production. The authors further showed that this pressure-induced superlattice formation is not restricted to spherical NPs. It also takes place for nanorods, forming 2D-hexagonal structures at high pressures and similar time scales as for spheres.[289]

4.6 Further approaches

Finally, we want to shortly present some new experimental approaches for the study of NP self-assembly that have not been addressed above because they do not fit into the categories. One example is the in situ assembly driven by an external field. Yu et al. measured 1-dodecanethiol capped silver (Ag) NP which are negatively charged due to surface adsorption of bromide anions (Br^-) during their synthesis.[305] This can be utilized for an electric field-driven assembly.[290] Using time- and space-resolved SAXS, a NP flux was found due to the electric field. In the following, nucleation and growth of superlattices took place within several minutes. Furthermore, a size-selection effect by the field was found. In this way the dispersity of the NPs in the superlattice was significantly reduced compared to the original size distribution. Therefore, superlattices of higher quality are obtained with tunable lattice constants depending on the strength of the electric field.

A different approach for studying interfacial assemblies of NPs was presented by Hu et al.[278,324] Instead of using a GISAXS geometry, they designed a sample chamber that provided a curvature-free liquid surface. In this way, the sample is measured in transmission

SAXS, which allows one to probe the assembly with high height resolution, only limited by the size of the focused X-ray beam.

A new possibility of studying the correlation of NP lattice and superlattice was presented recently by Deng et al.[325] They developed a 3D reciprocal space mapping for both SAXS and WAXS data from 3D supercrystals self-assembled from upconversion nanorods ($NaYF_4$:Yb,Er NRs). The assemblies showed both translational and orientational ordering, the latter especially between the rods and the superlattice. It was found that the supercrystals are built up from well-aligned nanorods and exhibit a polarization-dependent anisotropic optical response in two perpendicular directions.

Toso et al. introduced a multilayer diffraction method based on XRD for characterization of supercrystals build up from PbS platelets and $CsPbBr_3$ perovskite NPs.[326] One advantage of their method is that it does not need highly intense X-rays from synchrotron radiation sources. Therein, the NP were treated as scattering sources that form a so-called self-probing interferometer. This method enabled the determination of the nanocrystal size, interparticle spacing, and their fluctuations with high precision. For instance, an average NP displacement of well below 1 Å was reported demonstrating the high quality of the supercrystals. As discussed in an earlier section, perovskite NP supercrystals are among the few examples with experimentally demonstrated collective properties. An accessible accurate structural characterization by an XRD approach is therefore very valuable.

5 Conclusions and outlook

In this review we highlighted just a subset of the many excellent studies developing new and innovative approaches to study the self-assembly of NPs and self-assembled structures with diffraction, scattering, electron microscopy and combinations thereof. Structural studies of NP assemblies both in situ and ex situ will particularly benefit from the design of the next-generation synchrotron radiation sources. Such diffraction-limited storage rings are already in

operation at MAX-IV and ESRF-EBS, and many more will follow in the next years.[327–331] With an increase of brilliance, basically two characteristics will enable new type of experiments: (1) the accessible experimental time scale will be reduced to the range of nanoseconds, bridging the gap between storage-ring and Free-Electron Laser sources and (2) focusing down to few nanometers without intensity loss will become possible.[332] Thus, early stages of assemblies will be accessible, down to single-particle spatial resolution.

For some materials the perfection of the NP supercrystals already comes close to that of atomic crystals and this is especially important for the ongoing search for new collective properties which can even result in new and unexpected physics. Studies of structure and structure formation in NP supercrystals will help to improve the control of structure, scale and morphology and therefore also properties. The use of self-assembled structures in devices will certainly receive much and ongoing attention in the future and a lot of research remains to be done addressing the upscaling, reproducibility, mechanical properties, stability and other questions relevant for device integration. 2D and 3D printing strategies for NP supercrystals could play a major role in this respect. The huge variety of available NPs and ligands offers plenty of room for the discovery of exciting new structures and materials and facilitated by the progress in electron microscopy, diffraction and scattering techniques an ever-improving understanding of NP self-assembly will emerge. The field of adaptive and dynamic self-assembly as perfected by nature in living organisms is even more unexplored. We therefore expect that many exciting opportunities lie ahead. Last but not least, we would like to emphasize that interdisciplinary collaborations and communication are highly recommendable in research addressing self-assembly of NPs.

6 Acknowledgements

This work is supported by the Cluster of Excellence'Advanced Imaging of Matter' of the Deutsche Forschungsgemeinschaft (DFG)-EXC 2056-project ID 390715994.

Received: ((will be filled in by the editorial staff))
Revised: ((will be filled in by the editorial staff))
Published online: ((will be filled in by the editorial staff))

7 References

[1] C. P. Collier, T. Vossmeyer, J. R. Heath, *Annu. Rev. Phys. Chem.* **1998**, *49*, 371.
[2] M. A. Boles, M. Engel, D. V. Talapin, *Chem. Rev.* **2016**, *116*, 11220.
[3] G. Rainò, M. A. Becker, M. I. Bodnarchuk, R. F. Mahrt, M. V. Kovalenko, T. Stöferle, *Nature* **2018**, *563*, 671.
[4] N. S. Mueller, Y. Okamura, B. G. M. Vieira, S. Juergensen, H. Lange, E. B. Barros, F. Schulz, S. Reich, *Nature* **2020**, *583*, 780.
[5] C. L. Poyser, T. Czerniuk, A. Akimov, B. T. Diroll, E. A. Gaulding, A. S. Salasyuk, A. J. Kent, D. R. Yakovlev, M. Bayer, C. B. Murray, *ACS Nano* **2016**, *10*, 1163.
[6] C. R. Kagan, C. B. Murray, *Nat. Nanotechnol.* **2015**, *10*, 1013.
[7] X. Lan, M. Chen, M. H. Hudson, V. Kamysbayev, Y. Wang, P. Guyot-Sionnest, D. V. Talapin, *Nat. Mater.* **2020**, *19*, 323.
[8] J. F. Galisteo-López, M. Ibisate, R. Sapienza, L. S. Froufe-Pérez, Á. Blanco, C. López, *Adv. Mater.* **2011**, *23*, 30.
[9] A.-P. Hynninen, J. H. J. Thijssen, E. C. M. Vermolen, M. Dijkstra, A. van Blaaderen, *Nat. Mater.* **2007**, *6*, 202.
[10] J. Zhang, Z. Sun, B. Yang, *Curr. Opin. Colloid Interface Sci.* **2009**, *14*, 103.
[11] K. J. M. Bishop, C. E. Wilmer, S. Soh, B. A. Grzybowski, *Small* **2009**, *5*, 1600.
[12] G. M. Whitesides, B. Grzybowski, *Science* **2002**, *295*, 2418.
[13] B. A. Grzybowski, C. E. Wilmer, J. Kim, K. P. Browne, K. J. M. Bishop, *Soft Matter* **2009**, *5*, 1110.
[14] L. Wang, A. M. Urbas, Q. Li, *Adv. Mater.* **2020**, *32*, 1801335.
[15] H. Cölfen, M. Antonietti, *Angew. Chem., Int. Ed.* **2005**, *44*, 5576.
[16] Y. Min, M. Akbulut, K. Kristiansen, Y. Golan, J. Israelachvili, *Nat. Mater.* **2008**, *7*, 527.
[17] C. A. Silvera Batista, R. G. Larson, N. A. Kotov, *Science* **2015**, *350*, 1242477.
[18] S. Mehdizadeh Taheri, M. Michaelis, T. Friedrich, B. Förster, M. Drechsler, F. M. Römer, P. Bösecke, T. Narayanan, B. Weber, I. Rehberg, *Proc. Natl. Acad. Sci. U.S.A.* **2015**, *112*, 14484.
[19] S. Sun, *Adv. Mater.* **2006**, *18*, 393.
[20] M. Grzelczak, L. M. Liz-Marzán, R. Klajn, *Chem. Soc. Rev.* **2019**, *48*, 1342.
[21] K. A. Dawson, *Curr. Opin. Colloid Interface Sci.* **2002**, *7*, 218.
[22] V. J. Anderson, H. N. W. Lekkerkerker, *Nature* **2002**, *416*, 811.
[23] J. Hühn, C. Carrillo-Carrion, M. G. Soliman, C. Pfeiffer, D. Valdeperez, A. Masood, I. Chakraborty, L. Zhu, M. Gallego, Z. Yue, M. Carril, N. Feliu, A. Escudero, A. M. Alkilany, B. Pelaz, P. Del Pino, W. J. Parak, *Chem. Mater.* **2017**, *29*, 399.
[24] B. W. Goodfellow, Y. Yu, C. A. Bosoy, D.-M. Smilgies, B. A. Korgel, *J. Phys. Chem. Lett.* **2015**, *6*, 2406.
[25] A. Heuer-Jungemann, N. Feliu, I. Bakaimi, M. Hamaly, A. Alkilany, I. Chakraborty, A. Masood, M. F. Casula, A. Kostopoulou, E. Oh, K. Susumu, M. H. Stewart, I. L. Medintz, E. Stratakis, W. J. Parak, A. G. Kanaras, *Chem. Rev.* **2019**, *119*, 4819.
[26] T. Geyer, P. Born, T. Kraus, *Phys. Rev. Lett.* **2012**, *109*, 128302.
[27] S. Roke, O. Berg, J. Buitenhuis, A. van Blaaderen, M. Bonn, *Proc. Natl. Acad. Sci. U.S.A.* **2006**, *103*, 13310.

[28] M. Xu, K. H. Ku, Y. J. Lee, T. Kim, J. J. Shin, E. J. Kim, S.-H. Choi, H. Yun, B. J. Kim, *Macromolecules* **2021**, *54*, 3084.
[29] T. Pellegrino, S. Kudera, T. Liedl, A. Muñoz Javier, L. Manna, W. J. Parak, *Small* **2005**, *1*, 48.
[30] M. A. Boles, D. Ling, T. Hyeon, D. V. Talapin, *Nat. Mater.* **2016**, *15*, 141.
[31] T. Kister, D. Monego, P. Mulvaney, A. Widmer-Cooper, T. Kraus, *ACS Nano* **2018**, *12*, 5969.
[32] K. J. Si, Y. Chen, Q. Shi, W. Cheng, *Adv. Sci.* **2018**, *5*, 1700179.
[33] E. Auyeung, J. I. Cutler, R. J. Macfarlane, M. R. Jones, J. Wu, G. Liu, K. Zhang, K. D. Osberg, C. A. Mirkin, *Nat. Nanotechnol.* **2011**, *7*, 24.
[34] M. R. Jones, N. C. Seeman, C. A. Mirkin, *Science* **2015**, *347*, 1260901.
[35] R. J. Macfarlane, B. Lee, M. R. Jones, N. Harris, G. C. Schatz, C. A. Mirkin, *Science* **2011**, *334*, 204.
[36] D. J. Park, C. Zhang, J. C. Ku, Y. Zhou, G. C. Schatz, C. A. Mirkin, *Proc. Natl. Acad. Sci. U.S.A.* **2015**, *112*, 977.
[37] K. L. Young, M. B. Ross, M. G. Blaber, M. Rycenga, M. R. Jones, C. Zhang, A. J. Senesi, B. Lee, G. C. Schatz, C. A. Mirkin, *Adv. Mater.* **2014**, *26*, 653.
[38] D. Nykypanchuk, M. M. Maye, D. van der Lelie, O. Gang, *Nature* **2008**, *451*, 549.
[39] W. Liu, M. Tagawa, H. L. Xin, T. Wang, H. Emamy, H. Li, K. G. Yager, F. W. Starr, A. V. Tkachenko, O. Gang, *Science* **2016**, *351*, 582.
[40] T. Pellegrino, R. A. Sperling, A. P. Alivisatos, W. J. Parak, M. Osinski, *J. Biomed. Biotechnol.* **2007**, *2007*, 26796.
[41] W. J. Parak, T. Pellegrino, C. M. Micheel, D. Gerion, S. C. Williams, A. P. Alivisatos, *Nano Lett.* **2003**, *3*, 33.
[42] M. P. Pileni, *J. Phys. Chem. B* **2001**, *105*, 3358.
[43] C. B. Murray, C. R. Kagan, M. G. Bawendi, *Annu. Rev. Mater. Sci.* **2000**, *30*, 545.
[44] D. V. Talapin, E. V. Shevchenko, M. I. Bodnarchuk, X. Ye, J. Chen, C. B. Murray, *Nature* **2009**, *461*, 964.
[45] E. V. Shevchenko, D. V. Talapin, N. A. Kotov, S. O'Brien, C. B. Murray, *Nature* **2006**, *439*, 55.
[46] M. P. Pileni, *Bull. Chem. Soc. Jpn.* **2019**, *92*, 312.
[47] A. M. Kalsin, M. Fialkowski, M. Paszewski, S. K. Smoukov, K. J. M. Bishop, B. A. Grzybowski, *Science* **2006**, *312*, 420.
[48] Y. Du, H. Sheng, D. Astruc, M. Zhu, *Chem. Rev.* **2020**, *120*, 526.
[49] I. Chakraborty, T. Pradeep, *Chem. Rev.* **2017**, *117*, 8208.
[50] S. A. Claridge, A. W. Castleman, S. N. Khanna, C. B. Murray, A. Sen, P. S. Weiss, *ACS Nano* **2009**, *3*, 244.
[51] P. D. Jadzinsky, G. Calero, C. J. Ackerson, D. A. Bushnell, R. D. Kornberg, *Science* **2007**, *318*, 430.
[52] F. Fetzer, A. Maier, M. Hodas, O. Geladari, K. Braun, A. J. Meixner, F. Schreiber, A. Schnepf, M. Scheele, *Nat. Commun.* **2020**, *11*, 6188.
[53] X. Ye, C. Zhu, P. Ercius, S. N. Raja, B. He, M. R. Jones, M. R. Hauwiller, Y. Liu, T. Xu, A. P. Alivisatos, *Nat. Commun.* **2015**, *6*, 10052.
[54] R. A. Sperling, T. Liedl, S. Duhr, S. Kudera, M. Zanella, C.-A. J. Lin, W. H. Chang, D. Braun, W. J. Parak, *J. Phys. Chem. C* **2007**, *111*, 11552.
[55] X. Yu, D. Y. Lei, F. Amin, R. Hartmann, G. P. Acuna, A. Guerrero-Martínez, S. A. Maier, P. Tinnefeld, S. Carregal-Romero, W. J. Parak, *Nano Today* **2013**, *8*, 480.
[56] C. Yi, Y. Yang, B. Liu, J. He, Z. Nie, *Chem. Soc. Rev.* **2020**, *49*, 465.
[57] F. Schulz, O. Pavelka, F. Lehmkühler, F. Westermeier, Y. Okamura, N. S. Mueller, S. Reich, H. Lange, *Nat. Commun.* **2020**, *11*, 3821.
[58] D. Dong, R. Fu, Q. Shi, W. Cheng, *Nat. Protoc.* **2019**, *14*, 2691.
[59] P. J. Santos, P. A. Gabrys, L. Z. Zornberg, M. S. Lee, R. J. Macfarlane, *Nature* **2021**, *591*, 586.

[60] K. Wang, H. Ling, Y. Bao, M. Yang, Y. Yang, M. Hussain, H. Wang, L. Zhang, L. Xie, M. Yi, W. Huang, X. Xie, J. Zhu, *Adv. Mater.* **2018**, *30*, 1800595.
[61] D. V. Talapin, M. Engel, P. V. Braun, *MRS Bull.* **2020**, *45*, 799.
[62] C. R. Kagan, E. Lifshitz, E. H. Sargent, D. V. Talapin, *Science* **2016**, *353*, 885.
[63] M. R. Begley, D. S. Gianola, T. R. Ray, *Science* **2019**, *364*, eaav4299.
[64] J.-H. Choi, H. Wang, S. J. Oh, T. Paik, P. Sung, J. Sung, X. Ye, T. Zhao, B. T. Diroll, C. B. Murray, *Science* **2016**, *352*, 205.
[65] Y. Mai, A. Eisenberg, *Chem. Soc. Rev.* **2012**, *41*, 5969.
[66] R. B. Thompson, V. V. Ginzburg, M. W. Matsen, A. C. Balazs, *Macromolecules* **2002**, *35*, 1060.
[67] N. Yan, X. Liu, J. Zhu, Y. Zhu, W. Jiang, *ACS Nano* **2019**, *13*, 6638.
[68] S. Zhao, F. Caruso, L. Dähne, G. Decher, B. G. de Geest, J. Fan, N. Feliu, Y. Gogotsi, P. T. Hammond, M. C. Hersam, A. Khademhosseini, N. Kotov, S. Leporatti, Y. Li, F. Lisdat, L. M. Liz-Marzán, S. Moya, P. Mulvaney, A. L. Rogach, S. Roy, D. G. Shchukin, A. G. Skirtach, M. M. Stevens, G. B. Sukhorukov, P. S. Weiss, Z. Yue, D. Zhu, W. J. Parak, *ACS Nano* **2019**, *13*, 6151.
[69] D. Jishkariani, B. T. Diroll, M. Cargnello, D. R. Klein, L. A. Hough, C. B. Murray, B. Donnio, *J. Am. Soc. Chem.* **2015**, *137*, 10728.
[70] K. C. Elbert, D. Jishkariani, Y. Wu, J. D. Lee, B. Donnio, C. B. Murray, *Chem. Mater.* **2017**, *29*, 8737.
[71] K. C. Elbert, T. Vo, N. M. Krook, W. Zygmunt, J. Park, K. G. Yager, R. J. Composto, S. C. Glotzer, C. B. Murray, *ACS Nano* **2019**, *13*, 14241.
[72] D. García-Lojo, S. Gómez-Graña, V. F. Martín, D. M. Solís, J. M. Taboada, J. Pérez-Juste, I. Pastoriza-Santos, *ACS Appl. Mater. Interfaces* **2020**, *12*, 46557.
[73] D. M. Solís, J. M. Taboada, F. Obelleiro, L. M. Liz-Marzán, García de Abajo, F. Javier, *ACS Nano* **2014**, *8*, 7559.
[74] Y. Huang, D.-H. Kim, *Langmuir* **2011**, *27*, 13861.
[75] X. Ye, L. Jin, H. Caglayan, J. Chen, G. Xing, C. Zheng, V. Doan-Nguyen, Y. Kang, N. Engheta, C. R. Kagan, *ACS Nano* **2012**, *6*, 2804.
[76] G. Bodelón, V. Montes-García, V. López-Puente, E. H. Hill, C. Hamon, M. N. Sanz-Ortiz, S. Rodal-Cedeira, C. Costas, S. Celiksoy, I. Pérez-Juste, L. Scarabelli, A. La Porta, J. Pérez-Juste, I. Pastoriza-Santos, L. M. Liz-Marzán, *Nat. Mater.* **2016**, *15*, 1203.
[77] C. Hanske, G. González-Rubio, C. Hamon, P. Formentín, E. Modin, A. Chuvilin, A. Guerrero-Martínez, L. F. Marsal, L. M. Liz-Marzán, *J. Phys. Chem. C* **2017**, *121*, 10899.
[78] C. Hamon, S. Novikov, L. Scarabelli, L. Basabe-Desmonts, L. M. Liz-Marzán, *ACS Nano* **2014**, *8*, 10694.
[79] C. Hamon, M. Postic, E. Mazari, T. Bizien, C. Dupuis, P. Even-Hernandez, A. Jimenez, L. Courbin, C. Gosse, F. Artzner, V. Marchi-Artzner, *ACS Nano* **2012**, *6*, 4137.
[80] C. Matricardi, C. Hanske, J. L. Garcia-Pomar, J. Langer, A. Mihi, L. M. Liz-Marzán, *ACS Nano* **2018**, *12*, 8531.
[81] R. A. Sperling, W. J. Parak, *Phil. Trans. R. Soc. A* **2010**, *368*, 1333.
[82] M. G. Soliman, B. Pelaz, W. J. Parak, P. Del Pino, *Chem. Mater.* **2015**, *27*, 990.
[83] D. Doblas, T. Kister, M. Cano-Bonilla, L. González-García, T. Kraus, *Nano Lett.* **2019**, *19*, 5246.
[84] W. Han, Z. Lin, *Angew. Chem., Int. Ed.* **2012**, *51*, 1534.
[85] N. Vogel, M. Retsch, C.-A. Fustin, A. Del Campo, U. Jonas, *Chem. Rev.* **2015**, *115*, 6265.
[86] X. W. Gu, X. Ye, D. M. Koshy, S. Vachhani, P. Hosemann, A. P. Alivisatos, *Proc. Natl. Acad. Sci. U.S.A.* **2017**, *114*, 2836.
[87] L. Wu, J. J. Willis, I. S. McKay, B. T. Diroll, J. Qin, M. Cargnello, C. J. Tassone, *Nature* **2017**, *548*, 197.

[88] M. A. Schroer, F. Lehmkühler, J. Möller, H. Lange, G. Grübel, F. Schulz, *J. Phys. Chem. Lett.* **2018**, *9*, 4720.
[89] F. Lehmkühler, M. A. Schroer, V. Markmann, L. Frenzel, J. Möller, H. Lange, G. Grübel, F. Schulz, *Phys. Chem. Chem. Phys.* **2019**, *21*, 21349.
[90] M. Grzelczak, J. Vermant, E. M. Furst, L. M. Liz-Marzán, *ACS Nano* **2010**, *4*, 3591.
[91] M. Mayer, M. J. Schnepf, T. A. F. König, A. Fery, *Adv. Opt. Mater.* **2019**, *7*, 1800564.
[92] K. Thorkelsson, P. Bai, T. Xu, *Nano Today* **2015**, *10*, 48.
[93] V. Santhanam, J. Liu, R. Agarwal, R. P. Andres, *Langmuir* **2003**, *19*, 7881.
[94] Q. Guo, X. Teng, H. Yang, *Adv. Mater.* **2004**, *16*, 1337.
[95] J.-I. Park, W.-R. Lee, S.-S. Bae, Y. J. Kim, K.-H. Yoo, J. Cheon, S. Kim, *J. Phys. Chem. B* **2005**, *109*, 13119.
[96] B. O. Dabbousi, C. B. Murray, M. F. Rubner, M. G. Bawendi, *Chem. Mater.* **1994**, *6*, 216.
[97] K. Lambert, R. K. Capek, M. I. Bodnarchuk, M. V. Kovalenko, D. van Thourhout, W. Heiss, Z. Hens, *Langmuir* **2010**, *26*, 7732.
[98] V. Aleksandrovic, D. Greshnykh, I. Randjelovic, A. Frömsdorf, A. Kornowski, S. V. Roth, C. Klinke, H. Weller, *ACS Nano* **2008**, *2*, 1123.
[99] M. Sachan, N. D. Walrath, S. A. Majetich, K. Krycka, C.-C. Kao, *J. Appl. Phys.* **2006**, *99*, 08C302.
[100] A. Dong, J. Chen, P. M. Vora, J. M. Kikkawa, C. B. Murray, *Nature* **2010**, *466*, 474.
[101] K. J. Si, D. Sikdar, Y. Chen, F. Eftekhari, Z. Xu, Y. Tang, W. Xiong, P. Guo, S. Zhang, Y. Lu, Q. Bao, W. Zhu, M. Premaratne, W. Cheng, *ACS Nano* **2014**, *8*, 11086.
[102] X. M. Lin, H. M. Jaeger, C. M. Sorensen, K. J. Klabunde, *J. Phys. Chem. B* **2001**, *105*, 3353.
[103] T. P. Bigioni, X.-M. Lin, T. T. Nguyen, E. I. Corwin, T. A. Witten, H. M. Jaeger, *Nat. Mater.* **2006**, *5*, 265.
[104] X. Ye, C. Zhu, P. Ercius, S. N. Raja, B. He, M. R. Jones, M. R. Hauwiller, Y. Liu, T. Xu, A. P. Alivisatos, *Nat. Commun.* **2015**, *6*, 10052.
[105] K. Whitham, D.-M. Smilgies, T. Hanrath, *Chem. Mater.* **2018**, *30*, 54.
[106] T. Wen, S. A. Majetich, *ACS Nano* **2011**, *5*, 8868.
[107] W. H. Evers, B. Goris, S. Bals, M. Casavola, J. de Graaf, R. van Roij, M. Dijkstra, D. Vanmaekelbergh, *Nano Lett.* **2013**, *13*, 2317.
[108] A. Dong, X. Ye, J. Chen, C. B. Murray, *Nano Lett.* **2011**, *11*, 1804.
[109] Santanu Maiti, Alexander André, Rupak Banerjee, Jan Hagenlocher, Oleg Konovalov, Frank Schreiber, Marcus Scheele, *J. Phys. Chem. Lett.* **2018**, *9*, 739.
[110] F. Schulz, O. Pavelka, F. Lehmkühler, F. Westermeier, Y. Okamura, N. S. Mueller, S. Reich, H. Lange, *Nat. Commun.* **2020**, *11*, 3821.
[111] Kerong Deng, Zhishan Luo, Li Tan, Zewei Quan, *Chem. Soc. Rev.* **2020**, *49*, 6002.
[112] B. de Nijs, S. Dussi, F. Smallenburg, J. D. Meeldijk, D. J. Groenendijk, L. Filion, A. Imhof, A. van Blaaderen, M. Dijkstra, *Nat. Mater.* **2014**, *14*, 56.
[113] A. Plunkett, C. Eldridge, G. A. Schneider, B. Domènech, *J. Phys. Chem. B* **2020**, *124*, 11263.
[114] Y. Yang, B. Wang, X. Shen, L. Yao, L. Wang, X. Chen, S. Xie, T. Li, J. Hu, D. Yang, A. Dong, *J. Am. Soc. Chem.* **2018**, *140*, 15038.
[115] L. Nayak, S. Mohanty, S. K. Nayak, A. Ramadoss, *J. Mater. Chem. C* **2019**, *7*, 8771.
[116] E. Tekin, P. J. Smith, S. Hoeppener, A. M. J. van den Berg, A. S. Susha, A. L. Rogach, J. Feldmann, U. S. Schubert, *Adv. Funct. Mater.* **2007**, *17*, 23.
[117] C.-H. Su, H.-L. Chiu, Y.-C. Chen, M. Yesilmen, F. Schulz, B. Ketelsen, T. Vossmeyer, Y.-C. Liao, *Langmuir* **2019**, *35*, 3256.
[118] M. Boberl, M. V. Kovalenko, S. Gamerith, E. J. W. List, W. Heiss, *Adv. Mater.* **2007**, *19*, 3574.
[119] R. D. Farahani, M. Dubé, D. Therriault, *Adv. Mater.* **2016**, *28*, 5794.
[120] A. T. L. Tan, J. Beroz, M. Kolle, A. J. Hart, *Adv. Mater.* **2018**, *30*, 1803620.

[121] B. Domènech, A. T. L. Tan, H. Jelitto, E. Zegarra Berodt, M. Blankenburg, O. Focke, J. Cann, C. Cem Tasan, L. Colombi Ciacchi, M. Müller, K. P. Furlan, A. John Hart, G. A. Schneider, *Adv. Eng. Mater.* **2020**, *22*, 2000352.
[122] A. Dreyer, A. Feld, A. Kornowski, E. D. Yilmaz, H. Noei, A. Meyer, T. Krekeler, C. Jiao, A. Stierle, V. Abetz, H. Weller, G. A. Schneider, *Nat. Mater.* **2016**, *15*, 522.
[123] I. Cherniukh, G. Rainò, T. Stöferle, M. Burian, A. Travesset, D. Naumenko, H. Amenitsch, R. Erni, R. F. Mahrt, M. I. Bodnarchuk, M. V. Kovalenko, *Nature* **2021**, *593*, 535.
[124] M. Smeaton, I. E. Baggari, D. Balazs, T. Hanrath, L. Kourkoutis, *Microsc. Microanal.* **2020**, *26*, 2828.
[125] V. Gold, *The IUPAC Compendium of Chemical Terminology*, International Union of Pure and Applied Chemistry (IUPAC), Research Triangle Park, NC **2019**.
[126] M. Nespolo, *J. Appl. Crystallogr.* **2019**, *52*, 451.
[127] M. Niederberger, H. Cölfen, *Phys. Chem. Chem. Phys.* **2006**, *8*, 3271.
[128] Z. Ye, C. Li, Q. Chen, Y. Xu, S. E. J. Bell, *Nanoscale* **2021**, *13*, 5937.
[129] S. M. Rupich, E. V. Shevchenko, M. I. Bodnarchuk, B. Lee, D. V. Talapin, *J. Am. Soc. Chem.* **2010**, *132*, 289.
[130] J. Park, K. An, Y. Hwang, J.-G. Park, H.-J. Noh, J.-Y. Kim, J.-H. Park, N.-M. Hwang, T. Hyeon, *Nat. Mater.* **2004**, *3*, 891.
[131] T. Hyeon, S. S. Lee, J. Park, Y. Chung, H. B. Na, *J. Am. Soc. Chem.* **2001**, *123*, 12798.
[132] F. Lehmkühler, F. Schulz, M. A. Schroer, L. Frenzel, H. Lange, G. Grübel, *IUCrJ* **2018**, *5*, 354.
[133] F. Lehmkühler, G. Grübel, C. Gutt, *J. Appl. Crystallogr.* **2014**, *47*, 1315.
[134] F. Lehmkühler, F. Schulz, M. A. Schroer, L. Frenzel, H. Lange, G. Grübel, *J. Appl. Crystallogr.* **2019**, *52*, 777.
[135] S. C. Glotzer, M. J. Solomon, *Nat. Mater.* **2007**, *6*, 557.
[136] P. F. Damasceno, M. Engel, S. C. Glotzer, *Science* **2012**, *337*, 453.
[137] J. Gong, R. S. Newman, M. Engel, M. Zhao, F. Bian, S. C. Glotzer, Z. Tang, *Nat. Commun.* **2017**, *8*, 14038.
[138] C. R. Iacovella, S. C. Glotzer, *Nano Lett.* **2009**, *9*, 1206.
[139] D. Giuntini, S. Zhao, T. Krekeler, M. Li, M. Blankenburg, B. Bor, G. Schaan, B. Domènech, M. Müller, I. Scheider, M. Ritter, G. A. Schneider, *Sci. Adv.* **2021**, *7*, eabb6063.
[140] F. Schulz, S. Tober, H. Lange, *Langmuir* **2017**, *33*, 14437.
[141] T. Pellegrino, L. Manna, S. Kudera, T. Liedl, D. Koktysh, A. L. Rogach, S. Keller, J. Rädler, G. Natile, W. J. Parak, *Nano Lett.* **2004**, *4*, 703.
[142] L. Song, Y. Huang, Z. Nie, T. Chen, *Nanoscale* **2020**, *12*, 7433.
[143] N. Mac Fhionnlaoich, R. Qi, S. Guldin, *Langmuir* **2019**, *35*, 16605.
[144] Tao Li, Andrew J. Senesi, Byeongdu Lee, *Chem. Rev.* **2016**, *116*, 11128.
[145] P. Guyot-Sionnest, *J. Phys. Chem. Lett.* **2012**, *3*, 1169.
[146] K. Whitham, J. Yang, B. H. Savitzky, L. F. Kourkoutis, F. Wise, T. Hanrath, *Nat. Mater.* **2016**, *15*, 557.
[147] A. I. Ekimov, A. Efros, A. A. Onushchenko, *Solid State Commun.* **1985**, *56*, 921.
[148] S. Chen, *J. Mater. Chem.* **2007**, *17*, 4115.
[149] J. Dugay, R. P. Tan, M. Ibrahim, C. Garcia, J. Carrey, L.-M. Lacroix, P.-F. Fazzini, G. Viau, M. Respaud, *Phys. Rev. B* **2014**, *89*, 41406.
[150] S. Sun, C. B. Murray, D. Weller, L. Folks, A. Moser, *Science* **2000**, *287*, 1989.
[151] F. X. Redl, K.-S. Cho, C. B. Murray, S. O'Brien, *Nature* **2003**, *423*, 968.
[152] R. H. Dicke, *Phys. Rev.* **1954**, *93*, 99.
[153] A. Manjavacas, García de Abajo, F. J., P. Nordlander, *Nano Lett.* **2011**, *11*, 2318.
[154] A. E. Schlather, N. Large, A. S. Urban, P. Nordlander, N. J. Halas, *Nano Lett.* **2013**, *13*, 3281.

[155] A. Frisk Kockum, A. Miranowicz, S. de Liberato, S. Savasta, F. Nori, *Nat. Rev. Phys.* **2019**, *1*, 19.
[156] N. S. Mueller, B. G. M. Vieira, F. Schulz, P. Kusch, V. Oddone, E. B. Barros, H. Lange, S. Reich, *ACS Photonics* **2018**, *5*, 3962.
[157] N. S. Mueller, B. G. M. Vieira, D. Höing, F. Schulz, E. B. Barros, H. Lange, S. Reich, *Faraday Discuss.* **2019**, *214*, 159.
[158] Y. Zheng, X. Zhong, Z. Li, Y. Xia, *Part. Part. Syst. Charact.* **2014**, *31*, 266.
[159] N. S. Mueller, E. Pfitzner, Y. Okamura, G. Gordeev, P. Kusch, H. Lange, J. Heberle, F. Schulz, S. Reich, *ACS Nano* **2021**, *15*, 5523.
[160] D. Hoeing, F. Schulz, N. S. Mueller, S. Reich, H. Lange, *J. Chem. Phys.* **2020**, *152*, 64710.
[161] A. J. Nozik, M. C. Beard, J. M. Luther, M. Law, R. J. Ellingson, J. C. Johnson, *Chem. Rev.* **2010**, *110*, 6873.
[162] M. V. Kovalenko, L. Manna, A. Cabot, Z. Hens, D. V. Talapin, C. R. Kagan, V. I. Klimov, A. L. Rogach, P. Reiss, D. J. Milliron, *ACS Nano* **2015**, *9*, 1012.
[163] Z. Nie, A. Petukhova, E. Kumacheva, *Nat. Nanotechnol.* **2010**, *5*, 15.
[164] R. Tan, H. Zhu, C. Cao, O. Chen, *Nanoscale* **2016**, *8*, 9944.
[165] S. Mourdikoudis, R. M. Pallares, N. T. K. Thanh, *Nanoscale* **2018**, *10*, 12871.
[166] J. C. Meyer, C. O. Girit, M. F. Crommie, A. Zettl, *Nature* **2008**, *454*, 319.
[167] M. P. Blakeley, S. S. Hasnain, S. V. Antonyuk, *IUCrJ* **2015**, *2*, 464.
[168] Y. Yang, S. Liao, Z. Luo, R. Qi, N. Mac Fhionnlaoich, F. Stellacci, S. Guldin, *Nanoscale* **2020**, *12*, 12007.
[169] H. Borchert, E. V. Shevchenko, A. Robert, I. Mekis, A. Kornowski, G. Grübel, H. Weller, *Langmuir* **2005**, *21*, 1931.
[170] P. A. Midgley, R. E. Dunin-Borkowski, *Nat. Mater.* **2009**, *8*, 271.
[171] P. A. Midgley, M. Weyland, *Ultramicroscopy* **2003**, *96*, 413.
[172] S. Bals, B. Goris, L. M. Liz-Marzán, G. van Tendeloo, *Angew. Chem., Int. Ed.* **2014**, *53*, 10600.
[173] T. Altantzis, D. Zanaga, S. Bals, *EPL* **2017**, *119*, 38001.
[174] H. Wu, H. Friedrich, J. P. Patterson, Sommerdijk, Nico A. J. M., N. de Jonge, *Adv. Mater.* **2020**, *32*, 2001582.
[175] J. J. de Yoreo, N. A. J. M., Sommerdijk, *Nat. Rev. Mater.* **2016**, *1*, 16035.
[176] J. T. van Omme, H. Wu, H. Sun, A. F. Beker, M. Lemang, R. G. Spruit, S. P. Maddala, A. Rakowski, H. Friedrich, J. P. Patterson, H. H. Pérez Garza, *J. Mater. Chem. C* **2020**, *8*, 10781.
[177] Z. Ou, C. Liu, L. Yao, Q. Chen, *Acc. Mater. Res.* **2020**, *1*, 41.
[178] B. Luo, J. W. Smith, Z. Ou, Q. Chen, *Acc. Chem. Res.* **2017**, *50*, 1125.
[179] B. H. Kim, J. Yang, D. Lee, B. K. Choi, T. Hyeon, J. Park, *Adv. Mater.* **2018**, *30*, 1703316.
[180] X. Chen, C. Li, H. Cao, *Nanoscale* **2015**, *7*, 4811.
[181] F. M. Ross, *Science* **2015**, *350*, aaa9886.
[182] K. W. Urban, *Science* **2008**, *321*, 506.
[183] D. Su, *Green Energy Environ.* **2017**, *2*, 70.
[184] D. E. Jesson, S. J. Pennycook, *Proc. Natl. Acad. Sci. U.S.A.* **1995**, *449*, 273.
[185] P. D. Nellist, S. J. Pennycook, in *Advances in Imaging and Electron Physics*, Vol. 113 (Ed.: P. W. Hawkes), Elsevier **2000**, p. 147.
[186] M. A. Boles, D. V. Talapin, *J. Am. Soc. Chem.* **2014**, *136*, 5868.
[187] J. E. S. van der Hoeven, E. B. van der Wee, D. A. M. de Winter, M. Hermes, Y. Liu, J. Fokkema, M. Bransen, M. A. van Huis, H. C. Gerritsen, P. E. de Jongh, A. van Blaaderen, *Nanoscale* **2019**, *11*, 5304.
[188] M. Cantoni, L. Holzer, *MRS Bull.* **2014**, *39*, 354.
[189] D. Zanaga, F. Bleichrodt, T. Altantzis, N. Winckelmans, W. J. Palenstijn, J. Sijbers, B. de Nijs, M. A. van Huis, A. Sánchez-Iglesias, L. M. Liz-Marzán, *Nanoscale* **2016**, *8*, 292.

[190] K. J. Batenburg, S. Bals, J. Sijbers, C. Kübel, P. A. Midgley, J. C. Hernandez, U. Kaiser, E. R. Encina, E. A. Coronado, G. van Tendeloo, *Ultramicroscopy* **2009**, *109*, 730.
[191] D. Wang, T. Dasgupta, E. B. van der Wee, D. Zanaga, T. Altantzis, Y. Wu, G. M. Coli, C. B. Murray, S. Bals, M. Dijkstra, A. van Blaaderen, *Nat. Phys.* **2021**, *17*, 128.
[192] M. Bagiński, A. Pedrazo-Tardajos, T. Altantzis, M. Tupikowska, A. Vetter, E. Tomczyk, R. N. Suryadharma, M. Pawlak, A. Andruszkiewicz, E. Górecka, D. Pociecha, C. Rockstuhl, S. Bals, W. Lewandowski, *ACS Nano* **2021**, *15*, 4916.
[193] M. W. Tate, P. Purohit, D. Chamberlain, K. X. Nguyen, R. Hovden, C. S. Chang, P. Deb, E. Turgut, J. T. Heron, D. G. Schlom, D. C. Ralph, G. D. Fuchs, K. S. Shanks, H. T. Philipp, D. A. Muller, S. M. Gruner, *Microsc. Microanal.* **2016**, *22*, 237.
[194] C. Ophus, *Microsc. Microanal.* **2019**, *25*, 563.
[195] J. C. daSilva, M. A. Smeaton, T. A. Dunbar, Y. Xu, D. M. Balazs, L. F. Kourkoutis, T. Hanrath, *Nano Lett.* **2020**, *20*, 5267.
[196] Z. Wang, C. Schliehe, K. Bian, D. Dale, W. A. Bassett, T. Hanrath, C. Klinke, H. Weller, *Nano Lett.* **2013**, *13*, 1303.
[197] C. Schliehe, B. H. Juarez, M. Pelletier, S. Jander, D. Greshnykh, M. Nagel, A. Meyer, S. Foerster, A. Kornowski, C. Klinke, H. Weller, *Science* **2010**, *329*, 550.
[198] J. Novák, R. Banerjee, A. Kornowski, M. Jankowski, A. André, H. Weller, F. Schreiber, M. Scheele, *ACS Appl. Mater. Interfaces* **2016**, *8*, 22526.
[199] I. Y. Chen, J. Cimada daSilva, D. M. Balazs, M. A. Smeaton, L. F. Kourkoutis, T. Hanrath, P. Clancy, *ACS Nano* **2020**, *14*, 11431.
[200] C. Mueller, M. Harb, J. R. Dwyer, R. J. D. Miller, *J. Phys. Chem. Lett.* **2013**, *4*, 2339.
[201] K. Lim, Y. Bae, S. Jeon, K. Kim, B. H. Kim, J. Kim, S. Kang, T. Heo, J. Park, W. C. Lee, *Adv. Mater.* **2020**, *32*, 2002889.
[202] J. Park, K. Koo, N. Noh, J. H. Chang, J. Y. Cheong, K. S. Dae, J. S. Park, S. Ji, I.-D. Kim, J. M. Yuk, *ACS Nano* **2021**, *15*, 288.
[203] W. Yang, Y. Zhang, M. Hilke, W. Reisner, *Nanotechnology* **2015**, *26*, 315703.
[204] K. L. Jungjohann, J. E. Evans, J. A. Aguiar, I. Arslan, N. D. Browning, *Microsc. Microanal.* **2012**, *18*, 621.
[205] S. Keskin, P. Kunnas, N. de Jonge, *Nano Lett.* **2019**, *19*, 4608.
[206] M. N. Yesibolati, K. I. Mortensen, H. Sun, A. Brostrøm, S. Tidemand-Lichtenberg, K. Mølhave, *Nano Lett.* **2020**, *20*, 7108.
[207] T. A. J. Welling, S. Sadighikia, K. Watanabe, A. Grau-Carbonell, M. Bransen, D. Nagao, A. van Blaaderen, M. A. van Huis, *Part. Part. Syst. Charact.* **2020**, *37*, 2000003.
[208] S. Keskin, S. Besztejan, G. Kassier, S. Manz, R. Bücker, S. Riekeberg, H. K. Trieu, A. Rentmeister, R. J. D. Miller, *J. Phys. Chem. Lett.* **2015**, *6*, 4487.
[209] M. T. Proetto, A. M. Rush, M.-P. Chien, P. Abellan Baeza, J. P. Patterson, M. P. Thompson, N. H. Olson, C. E. Moore, A. L. Rheingold, C. Andolina, J. Millstone, S. B. Howell, N. D. Browning, J. E. Evans, N. C. Gianneschi, *J. Am. Soc. Chem.* **2014**, *136*, 1162.
[210] C. Wang, X. Chen, Y. Wu, Y. Li, S. Cheng, *J. Phys. Chem. C* **2020**, *124*, 26018.
[211] S. F. Tan, S. W. Chee, G. Lin, U. Mirsaidov, *Acc. Chem. Res.* **2017**, *50*, 1303.
[212] Y. Wang, X. Peng, A. Abelson, P. Xiao, C. Qian, L. Yu, C. Ophus, P. Ercius, L.-W. Wang, M. Law, H. Zheng, *Sci. Adv.* **2019**, *5*, eaaw5623.
[213] W. C. Lee, B. H. Kim, S. Choi, S. Takeuchi, J. Park, *J. Phys. Chem. Lett.* **2017**, *8*, 647.
[214] J. Lee, E. Nakouzi, M. Song, B. Wang, J. Chun, D. Li, *ACS Nano* **2018**, *12*, 12778.
[215] J. Kim, M. R. Jones, Z. Ou, Q. Chen, *ACS Nano* **2016**, *10*, 9801.
[216] Z. Ou, Z. Wang, B. Luo, E. Luijten, Q. Chen, *Nat. Mater.* **2020**, *19*, 450.
[217] Z. Ou, L. Yao, H. An, B. Shen, Q. Chen, *Nat. Commun.* **2020**, *11*, 4555.

[218] T. Narayanan, M. Sztucki, P. Van Vaerenbergh, J. Léonardon, J. Gorini, L. Claustre, F. Sever, J. Morse, P. Boesecke, *J. Appl. Crystallogr.* **2018**, *51*, 1511.
[219] Z. Jiang, B. Lee, *Appl. Phys. Rev.* **2021**, *8*, 11305.
[220] S. K. Sinha, Z. Jiang, L. B. Lurio, *Adv. Mater.* **2014**, *26*, 7764.
[221] M. Sutton, *C. R. Physique* **2008**, *9*, 657.
[222] M. Liebi, M. Georgiadis, A. Menzel, P. Schneider, J. Kohlbrecher, O. Bunk, M. Guizar-Sicairos, *Nature* **2015**, *527*, 349.
[223] W. H. de Jeu, *Basic X-Ray Scattering for Soft Matter*, OXFORD UNIV PR **2016**.
[224] T. Narayanan, O. Konovalov, *Materials* **2020**, *13*, 752.
[225] D. I. Svergun, M. H. J. Koch, *Rep. Progr. Phys.* **2003**, *66*, 1735.
[226] K. H. Kim, A. Späh, H. Pathak, F. Perakis, D. Mariedahl, K. Amann-Winkel, J. A. Sellberg, J. H. Lee, S. Kim, J. Park, K. H. Nam, T. Katayama, A. Nilsson, *Science* **2017**, *358*, 1589.
[227] M. C. Weidman, D.-M. Smilgies, W. A. Tisdale, *Nat. Mater.* **2016**, *15*, 775.
[228] F. Schulz, F. Westermeier, F. Dallari, V. Markmann, H. Lange, G. Grübel, F. Lehmkühler, *Adv. Mater. Interfaces* **2020**, *7*, 2000919.
[229] C. Krywka, C. Sternemann, M. Paulus, M. Tolan, C. Royer, R. Winter, *ChemPhysChem* **2008**, *9*, 2809.
[230] N. J. Brooks, B. L. L. E. Gauthe, N. J. Terrill, S. E. Rogers, R. H. Templer, O. Ces, J. M. Seddon, *Rev. Sci. Instrum.* **2010**, *81*, 64103.
[231] J. Möller, J. Léonardon, J. Gorini, R. Dattani, T. Narayanan, *Rev. Sci. Instrum.* **2016**, *87*, 125116.
[232] B. R. Pauw, J. S. Pedersen, S. Tardif, M. Takata, B. B. Iversen, *J. Appl. Crystallogr.* **2013**, *46*, 365.
[233] I. Bressler, B. R. Pauw, A. F. Thünemann, *J. Appl. Crystallogr.* **2015**, *48*, 962.
[234] C. Palencia, R. Seher, J. Krohn, F. Thiel, F. Lehmkühler, H. Weller, *Nanoscale* **2020**, *12*, 22928.
[235] D. Altamura, T. Sibillano, D. Siliqi, L. De Caro, C. Giannini, *Nanomater. Nanotechnol.* **2012**, *2*, 16.
[236] V. Saxena, G. Portale, *Nanomaterials* **2020**, *10*, 2240.
[237] M. Tolan, *X-Ray Scattering from Soft-Matter Thin Films. Materials Science and Basic Research: Materials Science and Basic Research*, Springer, Berlin, Heidelberg **1999**.
[238] Z. Kam, *Macromolecules* **1977**, *10*, 927.
[239] B. J. Ackerson, T. W. Taylor, N. A. Clark, *Phys. Rev. A* **1985**, *31*, 3183.
[240] D.K. Saldin, H.C. Poon, V.L. Shneerson, M. Howells, H.N. Chapman, R.A. Kirian, K.E. Schmidt, J.C.H. Spence, *Phys. Rev. Lett.* **2011**, *106*, 115501.
[241] D. K. Saldin, H. C. Poon, V. L. Shneerson, M. Howells, H. N. Chapman, R. A. Kirian, K. E. Schmidt, J. C. H. Spence, *Phys. Rev. B* **2010**, *81*, 174105.
[242] D. Starodub, A. Aquila, S. Bajt, M. Barthelmess, A. Barty, C. Bostedt, J.D. Bozek, N. Coppola, R.B. Doak, S.W. Epp, B. Erk, L. Foucar, L. Gumprecht, C.Y. Hampton, A. Hartmann, R. Hartmann, P. Holl, S. Kassemeyer, N. Kimmel, H. Laksmono, M. Liang, N.D. Loh, L. Lomb, A.V. Martin, K. Nass, C. Reich, D. Rolles, B. Rudek, A. Rudenko, J. Schulz, R.L. Shoeman, R.G. Sierra, H. Soltau, J. Steinbrener, F. Stellato, S. Stern, G. Weidenspointner, M. Frank, J. Ullrich, L. Strüder, I. Schlichting, H.N. Chapman, J.C.H. Spence, M.J. Bogan, *Nat. Commun.* **2012**, *3*, 1276.
[243] B. Pedrini, A. Menzel, M. Guizar-Sicairos, V.A. Guzenko, S. Gorelick, C. David, B.D. Patterson, R. Abela, *Nat. Commun.* **2013**, *4*, 1647.
[244] R. P. Kurta, J. J. Donatelli, C. H. Yoon, P. Berntsen, J. Bielecki, B. J. Daurer, H. DeMirci, P. Fromme, M. F. Hantke, F. R. Maia, others, *Phys. Rev. Lett.* **2017**, *119*, 158102.
[245] P. Wochner, C. Gutt, T. Autenrieth, T. Demmer, V. Bugaev, A. D. Ortiz, A. Duri, F. Zontone, G. Grübel, H. Dosch, *Proc. Natl. Acad. Sci. U.S.A.* **2009**, *106*, 11511.

[246] R. P. Kurta, M. Altarelli, E. Weckert, I. A. Vartanyants, *Phys. Rev. B* **2012**, *85*, 184204.
[247] M. Altarelli, R.P. Kurta, and I.A. Vartanyants, *Phys. Rev. B* **2010**, *82*, 104207.
[248] E. Malmerberg, C. A. Kerfeld, P. H. Zwart, *IUCrJ* **2015**, *2*, 309.
[249] T. Latychevskaia, G. F. Mancini, F. Carbone, *Sci. Rep.* **2015**, *5*, 16573.
[250] A. V. Martin, *IUCrJ* **2017**, *4*, 24.
[251] A C Y Liu, R F Tabor, L Bourgeois, M D de Jonge, S T Mudie, T C Petersen, *J. Stat. Mech: Theory Exp.* **2016**, *2016*, 54046.
[252] R. Su, K. A. Seu, D. Parks, J. J. Kan, E. E. Fullerton, S. Roy, S. D. Kevan, *Phys. Rev. Lett.* **2011**, *107*, 257204.
[253] I. A. Zaluzhnyy, R. P. Kurta, E. A. Sulyanova, O. Yu. Gorobtsov, A. G. Shabalin, A. V. Zozulya, A. P. Menushenkov, M. Sprung, A. Krówczyński, E. Górecka, B. I. Ostrovskii, I. A. Vartanyants, *Soft Matter* **2017**, *13*, 3240.
[254] I. A. Zaluzhnyy, R. P. Kurta, A. P. Menushenkov, B. I. Ostrovskii, I. A. Vartanyants, *Phys. Rev. E* **2016**, *94*, 30701.
[255] R. P. Kurta, B. I. Ostrovskii, A. Singer, O. Y. Gorobtsov, A. Shabalin, D. Dzhigaev, O. M. Yefanov, A. V. Zozulya, M. Sprung, I. A. Vartanyants, *Phys. Rev. E* **2013**, *88*, 44501.
[256] C. Gutt, L. Grodd, E. Mikayelyan, U. Pietsch, R. J. Kline, S. Grigorian, *J. Phys. Chem. Lett.* **2014**, *5*, 2335.
[257] R. P. Kurta, L. Grodd, E. Mikayelyan, O. Y. Gorobtsov, I. A. Zaluzhnyy, I. Fratoddi, I. Venditti, M. V. Russo, M. Sprung, I. A. Vartanyants, S. Grigorian, *Phys. Chem. Chem. Phys.* **2015**, *17*, 7404.
[258] A. C. Y. Liu, R. F. Tabor, M. D. de Jonge, S. T. Mudie, T. C. Petersen, *Proc. Natl. Acad. Sci. U.S.A.* **2017**, *114*, 10344.
[259] D. Mendez, H. Watkins, S. Qiao, K. S. Raines, T. J. Lane, G. Schenk, G. Nelson, G. Subramanian, K. Tono, Y. Joti, M. Yabashi, D. Ratner, S. Doniach, *IUCrJ* **2016**, *3*, 420.
[260] D. Mendez, T. J. Lane, J. Sung, J. Sellberg, C. Levard, H. Watkins, A. E. Cohen, M. Soltis, S. Sutton, J. Spudich, V. Pande, D. Ratner, S. Doniach, *Phil. Trans. R. Soc. B* **2014**, *369*, 20130315.
[261] V. Markmann, M. Dartsch, J. Valerio, L. Frenzel, I. Lokteva, M. Walther, F. Westermeier, G. Grübel, F. Lehmkühler, *Struct. Dyn.* **2020**, *7*, 54901.
[262] F. Lehmkühler, B. Hankiewicz, M. A. Schroer, L. Müller, B. Ruta, D. Sheyfer, M. Sprung, K. Tono, T. Katayama, M. Yabashi, T. Ishikawa, C. Gutt, G. Grübel, *Sci. Adv.* **2020**, *6*, eabc5916.
[263] R. P. Kurta, M. Altarelli, I. A. Vartanyants, *Adv. Chem. Phys.* **2016**, *161*, 1.
[264] F. Lehmkühler, B. Fischer, L. Müller, B. Ruta, G. Grübel, *J. Appl. Crystallogr.* **2016**, *49*, 2046.
[265] M. A. Schroer, C. Gutt, F. Lehmkühler, B. Fischer, I. Steinke, F. Westermeier, M. Sprung, G. Grübel, *Soft Matter* **2015**, *11*, 5465.
[266] I. A. Zaluzhnyy, R. P. Kurta, A. André, O. Y. Gorobtsov, M. Rose, P. Skopintsev, I. Besedin, A. V. Zozulya, M. Sprung, F. Schreiber, I. A. Vartanyants, M. Scheele, *Nano Lett.* **2017**, *17*, 3511.
[267] I. A. Zaluzhnyy, R. P. Kurta, N. Mukharamova, Y. Y. Kim, R. M. Khubbutdinov, D. Dzhigaev, V. V. Lebedev, E. S. Pikina, E. I. Kats, N. A. Clark, M. Sprung, B. I. Ostrovskii, I. A. Vartanyants, *Phys. Rev. E* **2018**, *98*, 52703.
[268] I. Lokteva, M. Koof, M. Walther, G. Grübel, F. Lehmkühler, *Small* **2019**, *15*, 1900438.
[269] N. Mukharamova, D. Lapkin, I. A. Zaluzhnyy, A. André, S. Lazarev, Y. Y. Kim, M. Sprung, R. P. Kurta, F. Schreiber, I. A. Vartanyants, M. Scheele, *Small* **2019**, *15*, 1904954.
[270] A. Maier, D. Lapkin, N. Mukharamova, P. Frech, D. Assalauova, A. Ignatenko, R. Khubbutdinov, S. Lazarev, M. Sprung, F. Laible, R. Löffler, N. Previdi, A. Bräuer, T. Günkel, M. Fleischer, F. Schreiber, I. A. Vartanyants, M. Scheele, *Adv. Mater.* **2020**, *32*, 2002254.
[271] S. Connolly, S. Fullam, B. Korgel, D. Fitzmaurice, *J. Am. Soc. Chem.* **1998**, *120*, 2969.
[272] Z. Lu, Y. Yin, *Chem. Soc. Rev.* **2012**, *41*, 6874.

[273] X. Huang, J. Zhu, B. Ge, K. Deng, X. Wu, T. Xiao, T. Jiang, Z. Quan, Y. C. Cao, Z. Wang, *J. Am. Soc. Chem.* **2019**, *141*, 3198.
[274] M. Agthe, T. S. Plivelic, A. Labrador, L. Bergström, G. Salazar-Alvarez, *Nano Lett.* **2016**, *16*, 6838.
[275] M. Kapuscinski, M. Agthe, Z.-P. Lv, Y. Liu, M. Segad, L. Bergström, *ACS Nano* **2020**, *14*, 5337.
[276] F. Montanarella, J. J. Geuchies, T. Dasgupta, P. T. Prins, C. van Overbeek, R. Dattani, P. Baesjou, M. Dijkstra, A. V. Petukhov, A. van Blaaderen, D. Vanmaekelbergh, *Nano Lett.* **2018**, *18*, 3675.
[277] Z.-P. Lv, M. Kapuscinski, L. Bergström, *Nat. Commun.* **2019**, *10*, 4228.
[278] J. Hu, E. W. C. Spotte-Smith, B. Pan, R. J. Garcia, C. Colosqui, I. P. Herman, *J. Phys. Chem. C* **2020**, *124*, 23949.
[279] M. Kapuscinski, P. Munier, M. Segad, L. Bergström, *Nano Lett.* **2020**, *20*, 7359.
[280] P. Siffalovic, E. Majkova, L. Chitu, M. Jergel, S. Luby, I. Capek, A. Satka, A. Timmann, S. V. Roth, *Small* **2008**, *4*, 2222.
[281] E. Josten, E. Wetterskog, A. Glavic, P. Boesecke, A. Feoktystov, E. Brauweiler-Reuters, U. Rücker, G. Salazar-Alvarez, T. Brückel, L. Bergström, *Sci. Rep.* **2017**, *7*, 2802.
[282] S. Narayanan, J. Wang, X.-M. Lin, *Phys. Rev. Lett.* **2004**, *93*, 135503.
[283] P.-W. Yang, S. Thoka, P.-C. Lin, C.-J. Su, H.-S. Sheu, M. H. Huang, U.-S. Jeng, *Langmuir* **2017**, *33*, 3253.
[284] B. W. Goodfellow, M. R. Rasch, C. M. Hessel, R. N. Patel, D.-M. M. Smilgies, B. A. Korgel, *Nano Lett.* **2013**, *13*, 5710.
[285] H. J. Kim, W. Wang, S. K. Mallapragada, D. Vaknin, *J. Phys. Chem. Lett.* **2021**, *12*, 1461.
[286] R. J. Macfarlane, B. Lee, H. D. Hill, A. J. Senesi, S. Seifert, C. A. Mirkin, *Proc. Natl. Acad. Sci. U.S.A.* **2009**, *106*, 10493.
[287] W. Cheng, M. J. Campolongo, J. J. Cha, S. J. Tan, C. C. Umbach, D. A. Muller, D. Luo, *Nat. Mater.* **2009**, *8*, 519.
[288] W. Cheng, M. R. Hartman, D.-M. Smilgies, R. Long, M. J. Campolongo, R. Li, K. Sekar, C.-Y. Hui, D. Luo, *Angew. Chem., Int. Ed.* **2010**, *49*, 380.
[289] M. A. Schroer, F. Lehmkühler, V. Markmann, L. Frenzel, J. Möller, H. Lange, G. Grübel, F. Schulz, *J. Phys. Chem. C* **2019**, *123*, 29994.
[290] Y. Yu, D. Yu, C. A. Orme, *Nano Lett.* **2017**, *17*, 3862.
[291] A. Huerre, F. Cacho-Nerin, V. Poulichet, C. E. Udoh, M. de Corato, V. Garbin, *Langmuir* **2018**, *34*, 1020.
[292] K. Whitham, T. Hanrath, *J. Phys. Chem. Lett.* **2017**, *8*, 2623.
[293] J. J. Geuchies, C. van Overbeek, W. H. Evers, B. Goris, A. de Backer, A. P. Gantapara, F. T. Rabouw, J. Hilhorst, J. L. Peters, O. Konovalov, A. V. Petukhov, M. Dijkstra, L. D. A. Siebbeles, S. van Aert, S. Bals, D. Vanmaekelbergh, *Nat. Mater.* **2016**, *15*, 1248.
[294] J. J. Geuchies, G. Soligno, E. Geraffy, C. P. Hendrikx, C. van Overbeek, F. Montanarella, M. R. Slot, O. V. Konovalov, A. V. Petukhov, D. Vanmaekelbergh, *Commun. Chem.* **2020**, *3*, 28.
[295] D. M. Balazs, T. A. Dunbar, D.-M. Smilgies, T. Hanrath, *Langmuir* **2020**, *36*, 6106.
[296] K. Bian, J. J. Choi, A. Kaushik, P. Clancy, D.-M. Smilgies, T. Hanrath, *ACS Nano* **2011**, *5*, 2815.
[297] I. Lokteva, M. Walther, M. Koof, G. Grübel, F. Lehmkühler, *Rev. Sci. Instrum.* **2019**, *90*, 36103.
[298] B. Lee, K. Littrell, Y. Sha, E. V. Shevchenko, *J. Am. Soc. Chem.* **2019**, *141*, 16651.
[299] X. Huang, J. Zhu, B. Ge, F. Gerdes, C. Klinke, Z. Wang, *J. Am. Soc. Chem.* **2021**, *143*, 4234.
[300] M. Corricelli, D. Altamura, M. L. Curri, T. Sibillano, D. Siliqi, A. Mazzone, N. Depalo, E. Fanizza, D. Zanchet, C. Giannini, M. Striccoli, *CrystEngComm* **2014**, *16*, 9482.
[301] S. Maiti, S. Maiti, A. Maier, J. Hagenlocher, A. Chumakov, F. Schreiber, M. Scheele, *J. Phys. Chem. C* **2018**, *123*, 1519.

[302] A. YousefiAmin, N. A. Killilea, M. Sytnyk, P. Maisch, K. C. Tam, H.-J. Egelhaaf, S. Langner, T. Stubhan, C. J. Brabec, T. Rejek, M. Halik, K. Poulsen, J. Niehaus, A. Köck, W. Heiss, *ACS Nano* **2019**, *13*, 2389.

[303] B. Li, K. Bian, X. Zhou, P. Lu, S. Liu, I. Brener, M. Sinclair, T. Luk, H. Schunk, L. Alarid, P. G. Clem, Z. Wang, H. Fan, *Sci. Adv.* **2017**, *3*, e1602916.

[304] F. Pietra, F. T. Rabouw, W. H. Evers, D. V. Byelov, A. V. Petukhov, C. de Mello Donegá, D. Vanmaekelbergh, *Nano Lett.* **2012**, *12*, 5515.

[305] Y. Yu, D. Yu, B. Sadigh, C. A. Orme, *Nat. Commun.* **2018**, *9*, 4211.

[306] M. Schwartzkopf, S.-J. Wöhnert, V. Waclawek, N. Carstens, A. Rothkirch, J. Rubeck, M. Gensch, J. Drewes, O. Polonskyi, T. Strunskus, A. M. Hinz, S. J. Schaper, V. Körstgens, P. Müller-Buschbaum, F. Faupel, S. V. Roth, *Nanoscale Horiz* **2021**, *6*, 132.

[307] M. C. Weidman, Q. Nguyen, D.-M. Smilgies, W. A. Tisdale, *Chem. Mater.* **2018**, *30*, 807.

[308] W. Chen, H. Tang, N. Li, M. A. Scheel, Y. Xie, D. Li, V. Körstgens, M. Schwartzkopf, S. V. Roth, K. Wang, X. W. Sun, P. Peter Müller-Buschbaum, *Nanoscale Horiz* **2020**, *5*, 880.

[309] I. Lokteva, M. Koof, M. Walther, G. Grübel, F. Lehmkühler, *J. Phys. Chem. Lett.* **2019**, *10*, 6331.

[310] A. P. Gantapara, J. de Graaf, R. van Roij, M. Dijkstra, *Phys. Rev. Lett.* **2013**, *111*, 15501.

[311] P. Sønderby, C. Söderberg, C. G. Frankær, G. Peters, J. T. Bukrinski, A. Labrador, T. S. Plivelic, P. Harris, *J. Synchrotron Rad.* **2020**, *27*, 396.

[312] Y. Liu, M. Agthe, M. Salajková, K. Gordeyeva, V. Guccini, A. Fall, G. Salazar-Alvarez, C. Schütz, L. Bergström, *Nanoscale* **2018**, *10*, 18113.

[313] Q. Shi, W. Di, D. Dong, L. W. Yap, L. Li, D. Zang, W. Cheng, *ACS Nano* **2019**, *13*, 5243.

[314] X. Wang, L. Wu, G. Wang, G. Chen, *Nano Lett.* **2019**, *19*, 8225.

[315] J. Lacava, P. Born, T. Kraus, *Nano Lett.* **2012**, *12*, 3279.

[316] T. Kister, M. Mravlak, T. Schilling, T. Kraus, *Nanoscale* **2016**, *8*, 13377.

[317] S. Saeki, N. Kuwahara, M. Nakata, M. Kaneko, *Polymer* **1976**, *17*, 685.

[318] R. D. Lundberg, F. E. Bailey, R. W. Callard, *J. Polym. Sci. A-1 Polym. Chem.* **1966**, *4*, 1563.

[319] D. Zámbó, G. Z. Radnóczi, A. Deák, *Langmuir* **2015**, *31*, 2662.

[320] J. SantaLucia, *Proc. Natl. Acad. Sci. U.S.A.* **1998**, *95*, 1460.

[321] F. Bai, K. Bian, X. Huang, Z. Wang, H. Fan, *Chem. Rev.* **2019**, *119*, 7673.

[322] M. A. Schroer, F. Schulz, F. Lehmkühler, J. Möller, A. J. Smith, H. Lange, T. Vossmeyer, G. Grübel, *J. Phys. Chem. C* **2016**, *120*, 19856.

[323] F. Schulz, J. Möller, F. Lehmkühler, A. J. Smith, T. Vossmeyer, H. Lange, G. Grübel, M. A. Schroer, *Parti. Part. Sys. Charact.* **2017**, *35*, 1700319.

[324] J. Hu, E. W. C. Spotte-Smith, B. Pan, I. P. Herman, *J. Nanoparticle Res.* **2019**, *21*, 71.

[325] K. Deng, X. Huang, Y. Liu, L. Xu, R. Li, J. Tang, Q. Lei, R. Ni, C. Li, Y. S. Zhao, H. Xu, Z. Wang, Z. Quan, *Nano Lett.* **2020**, *20*, 7367.

[326] S. Toso, D. Baranov, D. Altamura, F. Scattarella, J. Dahl, X. Wang, S. Marras, A. P. Alivisatos, A. Singer, C. Giannini, L. Manna, *ACS Nano* **2021**, *15,* 6243.

[327] M. Eriksson, J. F. van der Veen, C. Quitmann, *J. Synchrotron Rad.* **2014**, *21*, 837.

[328] C. G. Schroer, I. Agapov, W. Brefeld, R. Brinkmann, Y.-C. Chae, H.-C. Chao, M. Eriksson, J. Keil, X. Nuel Gavaldà, R. Röhlsberger, O. H. Seeck, M. Sprung, M. Tischer, R. Wanzenberg, E. Weckert, *J. Synchrotron Rad.* **2018**, *25*, 1277.

[329] R. Hettel, *J. Synchrotron Rad.* **2014**, *21*, 843.

[330] E. Weckert, *IUCrJ* **2015**, *2*, 230.

[331] P. Raimondi, *Synchrotron Radiat. News* **2016**, *29*, 8.

[332] C. G. Schroer, H. DESY Dt. Elektr.-Synchr., *PETRA IV: upgrade of PETRA III to the Ultimate 3D X-ray microscope. Conceptual Design Report*, Deutsches Elektronen-Synchrotron DESY, Hamburg **2019**.

Florian Schulz is group leader and senior scientist at the Institute of Nanostructure and Solid State Physics of the University of Hamburg. He obtained his PhD in 2014 in the group of Prof. Horst Weller, followed by a PostDoc in the group of Prof. Holger Lange. His research interests include the synthesis, surface chemistry and self-assembly of nanoparticles, especially gold nanoparticles, and studying their properties with small-angle X-ray scattering, electron microscopy and ultrafast spectroscopy.

Irina Lokteva is a research scientist at Deutsches Elektronen-Synchrotron DESY and the Hamburg Centre for Ultrafast Imaging (CUI), University of Hamburg, Germany. In 2010, she obtained her Ph.D. from Energy and Semiconductor Research Laboratory, Department of Physics, University of Oldenburg, Germany. Her current research interests include investigation of the in situ self-assembly of colloidal nanoparticles with Small-Angle X-ray Scattering and X-ray Cross-Correlation Analysis.

Felix Lehmkühler is a senior scientist in the Photon Science division at Deutsches Elektronen-Synchrotron DESY in Hamburg, Germany. He obtained his Ph.D. in physics at TU Dortmund in 2010. Felix' research interests cover X-ray studies on the structure and dynamics of soft matter, nanomaterials and water-based systems, with special attention on developing X-ray scattering methods using the latest generation of free-electron laser and synchrotron radiation sources.

Self-assembly of nanoparticles continues to fascinate researchers across various fields. Developments in electron microscopy and synchrotrons as sources of X-rays stimulate innovative experimental approaches to study self-assembly and self-assembled materials ex situ and in situ with ever increasing temporal and spatial resolution. Based on an introduction of nanoparticle self-assembly and important characterization techniques we highlight recent developments and interesting studies.

Florian Schulz,* Irina Lokteva, Wolfgang J. Parak, and Felix Lehmkühler*

Recent Notable Approaches to Study Self-Assembly of Nanoparticles with X-ray Scattering and Electron Microscopy